FEDERAL UNIVERSITY OF TECHNOLOGY - PARANÁ
POSTGRADUATE PROGRAM IN MECHANICAL AND MATERIALS ENGINEERING

TIAGO AUGUSTO DE MOURA VIEIRA

EFEITOS DA VISCOSIDADE NA TRANSIÇÃO DE PADRÕES DE ESCOAMENTO BIFÁSICO LÍQUIDO-SÓLIDO EM TUBULAÇÕES HORIZONTAIS

Dissertation

CURITIBA

2020

TIAGO AUGUSTO DE MOURA VIEIRA

EFEITOS DA VISCOSIDADE NA TRANSIÇÃO DE PADRÕES DE ESCOAMENTO BIFÁSICO LÍQUIDO-SÓLIDO EM TUBULAÇÕES HORIZONTAIS

Effects of Fluid Viscosity in Liquid-Solid Flow Pattern Transition in Horizontal Pipelines

MSc thesis presented to the Postgraduate Program in Mechanical and Materials Engineering from the Federal University of Technology – Paraná, as partial fulfillment of the Master's degree in Engineering.

Concentration Area: Thermal Engineering.

Supervisor: Prof. Dr. Admilson Teixeira Franco.

Co-Supervisor: Prof. Dr. Eduardo Matos Germer.

CURITIBA
2020

Ministério da Educação
Universidade Tecnológica Federal do Paraná
Câmpus Curitiba

TIAGO AUGUSTO DE MOURA VIEIRA

EFEITOS DA VISCOSIDADE NA TRANSIÇÃO DE PADRÕES DE ESCOAMENTO BIFÁSICO LÍQUIDO-SÓLIDO EM TUBULAÇÕES HORIZONTAIS

Trabalho de pesquisa de mestrado apresentado como requisito para obtenção do título de Mestre Em Engenharia da Universidade Tecnológica Federal do Paraná (UTFPR). Área de concentração: Engenharia Térmica.

Data de aprovação: 26 de Novembro de 2020

Prof Admilson Teixeira Franco, Doutorado - Universidade Tecnológica Federal do Paraná

Prof Marcelo Risso Errera, Doutorado - Universidade Federal do Paraná (Ufpr)

Prof Moises Alves Marcelino Neto, Doutorado - Universidade Tecnológica Federal do Paraná

Documento gerado pelo Sistema Acadêmico da UTFPR a partir dos dados da Ata de Defesa em 04/12/2020.

RESUMO

A remoção de cascalhos é um problema de grande preocupação nas operações de perfuração de poços de petróleo, uma vez que a limpeza deficiente do poço pode levar a vários problemas operacionais, como redução da vida útil das brocas e aprisionamento da tubulação. Diferentes configurações podem ser observadas durante os escoamentos líquido-sólido, conhecidos como padrões de escoamento, e é essencial entender as condições em que cada configuração é formada, visando evitar problemas operacionais. Uma bancada experimental foi projetada para desenvolver um mapa de padrão de escoamento e foi montada no CERNN/UTFPR. Três fluidos de trabalho foram empregados: água, e misturas de água-glicerina com 40% e 60% em peso, permitindo uma variação de viscosidade ao longo dos experimentos. Partículas de uréia com tamanho médio de 1,44 mm e massa específica de 1480 kg/m³ foram usadas para representar a fase discreta. A avaliação dos padrões de escoamento foi desenvolvida através da medição da queda de pressão e visualização do escoamento. Com base no mapa do padrão de escoamento, afirmou-se que a viscosidade realmente afeta a transição entre os padrões. De forma geral, fluidos de maior viscosidade requerem menor velocidade média para a transição, impondo menores valores de queda de pressão. O efeito descrito é mais significativo para a transição entre o leito móvel e os escoamentos heterogêneos do que para a transição do leito estacionário para o leito móvel. A influência é intensificada para o primeiro caso devido à erosão do leito formado por partículas planas. A água não conseguiu suspender partículas por erosão por impacto, devido à pequena área de seção transversal das partículas, que é a causa mais relevante da erosão do leito para fluidos de baixa viscosidade. Por outro lado, a alta viscosidade intensifica a erosão por cisalhamento, que não é muito afetada pelas partículas planas. Por fim, foi desenvolvida uma correlação, permitindo a determinação da queda de pressão em função do número de Reynolds e da viscosidade cinemática dos fluidos. Os resultados da correlação estiveram em concordância satisfatória com os dados experimentais.

Palavras-Chave: Escoamento bifásico sólido-líquido, experimental, padrão de escoamento, viscosidade.

ABSTRACT

Cuttings removal is a problem of significant concern in drilling operations since poor hole cleaning may lead to several operational problems, such as reducing bits life and stuck pipe. Different configurations may be observed during liquid-solid flows, known as flow patterns, and it is essential to understand the conditions in which each configuration is formed, aiming to avoid those operational problems. An experimental rig was designed to develop a flow pattern map and was be assembled in CERNN/UTFPR. Three working fluids were employed: water, water-glycerin 40%wt, and water-glycerin 60%wt mixtures allowing a viscosity variation over the experiments. Urea particles of the average size of 1.44 mm and a specific mass of 1480 kg/m³ were used as the discreet phase. The evaluation of the flow patterns was developed through pressure drop measurement and flow visualization. Based on the flow pattern map, it was stated that the viscosity indeed affects the flow pattern transition. The general statement was that higher viscosity fluids required smaller mean velocity for the transition, which happened at lower pressure drop values. The effect described is more significant for the transition between the moving bed and heterogeneous flows than for stationary bed to moving bed transition. The influence is intensified for the first case due to the bed erosion of flat particles. The water could not suspend particles through impact erosion due to the small cross-section area of the flat-shaped particles, which is the most relevant bed erosion cause for low viscosity fluids. On the other hand, the high viscosity intensifies the shear erosion, which is not greatly affected by the flat-shaped particles. Finally, a correlation was developed, allowing the pressure drop determination as a function of the Reynolds number and the fluids' kinematic viscosity. The results of the correlation were in satisfactory agreement with experimental data.

Keywords: Liquid-solid flow, experimental, flow pattern, fluid viscosity.

CONTENT

LIST OF FIGURES

LIST OF TABLES

LIST OF SYMBOLS

Roman Letters

A	Cross-section area	[m²]
B	Generic constant for equation fitting.	
C	Generic constant for equation fitting.	
C_D	Drag Coefficient	[-]
C_s	Solids Concentration	[-]
D	Pipeline diameter	[m]
D_h	Hydraulic diameter	[m]
d_p	Particle diameter	[m]
e	Pipeline roughness	[m]
Eu	Euler's number	[-]
f	Friction factor	
F_D	Drag force	[N]
Fr	Froude's number	[-]
F_w	Particle weight	[N]
g	Acceleration due to gravity	[m/s²]
K	Minor losses constant	
L	Pipeline length	[m]
L_e	Pipeline length development	[m]
M	Generic constant for equation fitting.	
n	Generic constant for equation fitting.	
Δp	Pressure gradient	[Pa]
P		
Q	Volumetric flow rate	[m³/s]
Re	Reynolds number	[-]
T	Temperature	[ºC]

Δt	Time interval	[s]
u_f	Fluid average velocity	[m/s]
$\mathbf{u_f}$	Vector of fluid velocity	[m/s]
u_m	Mixture mean velocity	[m/s]
$\bar{x}$	Average of measured values	
x_j	Generic measured value	

Greek Letters

Δ	Gradient	
δ	Experimental uncertainty	
ε	Volumetric fraction	[-]
μ_ϕ	Fluid dynamic viscosity	[Pa.s]
ν	Fluid kinematic viscosity	[m²/s]
Π_i	Generic pi-group	
ρ_f	Fluids density	[Kg/m³]
ρ_s	Solids density	[Kg/m³]
τ	Shear stress	[Pa]
ϕ	Reduced function	

Subscript

H	Heterogeneous suspension
Hmb	Moving bed to heterogeneous suspension boundary
S	Solid
P	Particle
F	Fluid

1. INTRODUCTION

1.1. Context

The national and international economic scenarios are greatly affected by the oil and gas industry. According to the Brazilian National Agency of Petroleum, Natural Gas and Biofuels (ANP), the oil and gas sector represented 13% of the national gross domestic product in 2018 (ANP, 2018).

Due to the increasing demand for oil and gas, exploitation has been conducted in more challenging conditions. Brazilian oil and gas production is carried almost exclusively by offshore facilities, representing around 96% of the Brazilian production in 2018 (ANP, 2018).

Offshore operations are much more challenging than onshore due to the difficulty in maintaining and assisting in the open sea (FREITAS et al., 2007). Also, reservoirs may reach depths up to 5,000 m below sea level (CEDRO, 2014), significantly increasing the operation complexity. The seabed and rock formations must be drilled under those sensitive conditions to reach the reservoirs. The drilling technique most employed for this matter is the rotary drilling (Bourgoyne et al., 1991), consisting of a rock cutting tool, known as a drill bit, to which rotation and a downward force are imposed in order to fracture the rock formation through shear and compression (Nazari et al., 2010).

Depending on the reservoir and rock formation conditions, directional drilling may be employed (ADITC, 2015). This drilling technique allows the orientation of the drilling bit path to avoid hard rock formations. In this case, horizontal or low angled sections will be present in the pipeline. The differences between conventional vertical drilling and directional drilling are illustrated in Figure 1.

Figure 1 – Vertical and directional drilling techniques illustration.

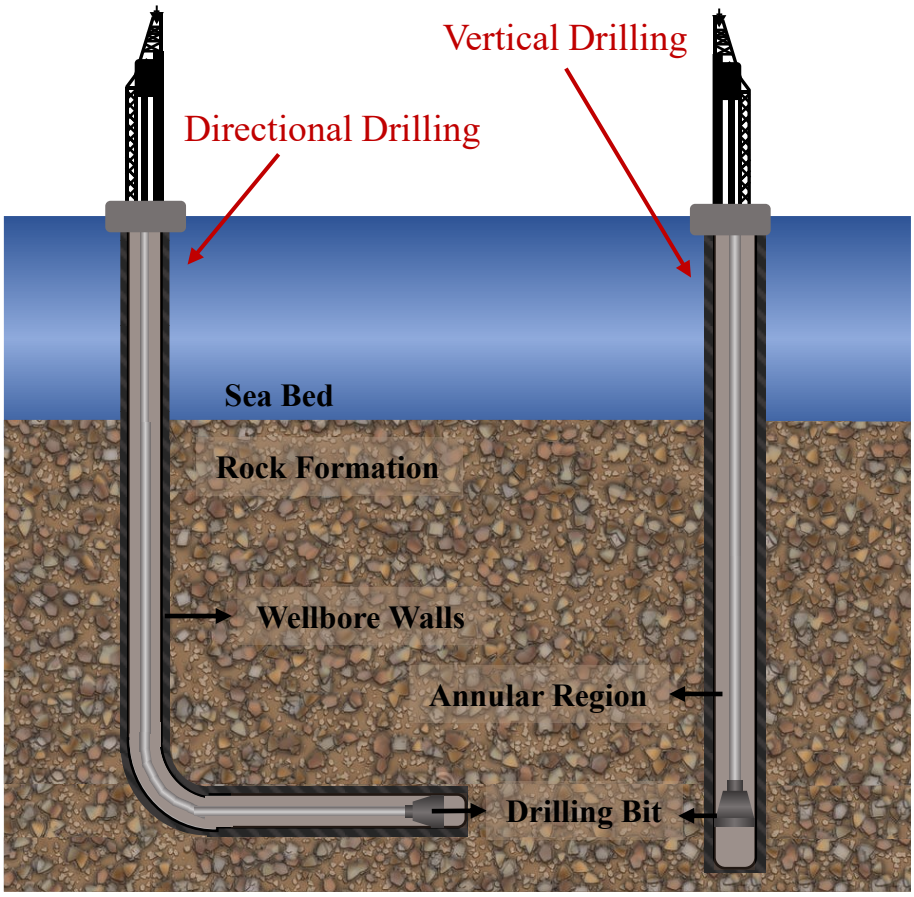

(Source: Author)

1.2. Problem Characterization

Drilling fluids are employed in drilling processes in order to establish a wellbore hydrostatic balance by ensuring that the pressure on the borehole walls is within an operational window, to lubricate and cool the drill bit, and, among other functions, to carry the cuttings resulting from the drilling process to the surface (Ragouilliaux et al., 2006). The fluid is generally pumped through the drill string, passes through the bit nozzle, and returns through the annular region, as illustrated in Figure 2.

Figure 2 – Illustration of fluid injection in drilling operations.

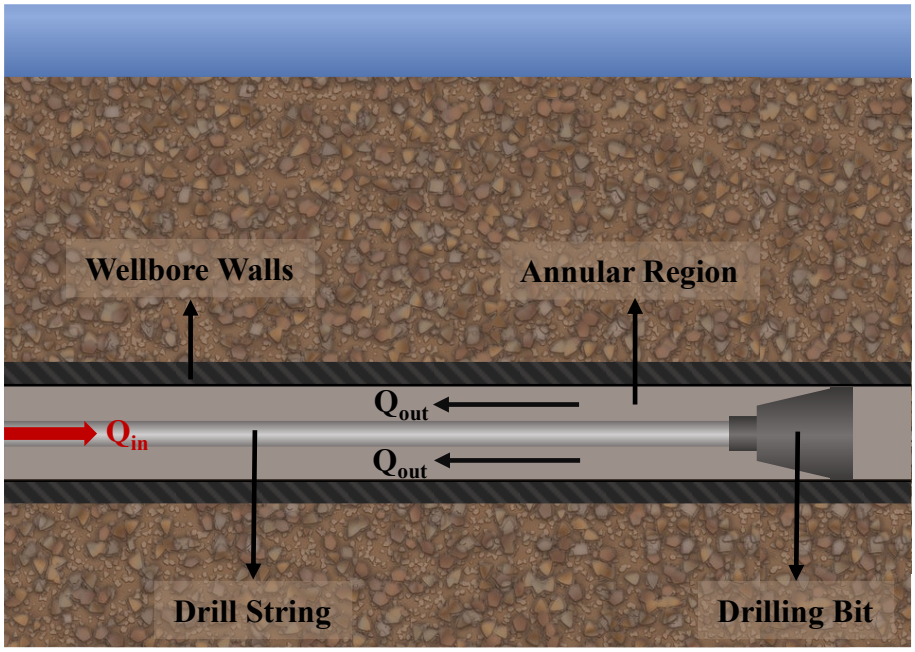

(Source: author)

Ensuring efficient cuttings transport is a significant concern over the drilling process since poor hole cleaning may raise the drilling costs and lead to problems such as stuck pipe, increase the drilling torque, reduce the drill bit's life and decrease the rate of penetration (Amanna et al., 2016). Therefore, it is vital to understand the physical mechanisms present in the biphasic settling flow and the operational variables affecting cuttings transport.

The gravitational force on the solid element must be overcome by the drilling fluid action over it in order to remove the cuttings (Amanna et al., 2016). Consequently, the operational parameters' effects over the cuttings's transport efficiency are highly dependent on the well inclination (Hussaini and Azar, 1983; Larsen et al., 1997). Some of the most relevant operational parameters regarding hole cleaning are the rate of penetration, drill string rotation, pipeline inclination, volumetric flow rate, and particle and fluid properties (Nazari et al., 2010). Several studies have investigated the cuttings removal efficiency evaluating each operational parameter's performance and its sensitivity to the pipeline inclination. It was concluded that fluid properties (such as density, viscosity, and other rheological properties) affected the cuttings removal more at

low angled or horizontal wells, while the volumetric flow rate increased the hole cleaning efficiency at high angled or vertical wells (Hussaini and Azar, 1983; Larsen et al., 1997).

Due to the solid particles' settling tendency, the liquid and solid phases will be arranged in different configurations, known as flow patterns[1]. The flow pattern formation depends on each operational variable's combination to which the system is subjected (Doron and Barnea, 1995; Kelessidis and Bandelis, 2005).

The pressure drop for biphasic liquid-solid flows is highly dependent on the flow pattern in which the system is operating (Doron et al., 1987; Peker and Helvaci, 2011). Therefore, it is desirable to determine the flow configuration that an industrial pipeline is subjected (Capecelatro and Desjardins, 2013; Doron and Barnea, 1995; Turian and Yuan, 1977). Also, avoiding the formation of a cuttings bed layer at the bottom of the pipeline may prevent the system's blockage (Capecelatro and Desjardins, 2013). However, the detection of those patterns is developed through visualization (Doron et al., 1987; Doron and Barnea, 1996, 1995; Kelessidis and Bandelis, 2005), which is not viable in most industrial applications, especially during offshore drilling. Therefore, there is an interest in developing flow patterns and pressure drop predicting tools for liquid-solid flows.

Flow pattern maps were initially employed for liquid-gas flows (Doron and Barnea, 1996). Later, these maps were developed for liquid-solid flow pattern prediction as a function of the mixture mean velocity, particle density, solids concentration, and particle and pipe diameters (Doron and Barnea, 1996). However, the flow pattern maps were developed employing only water as the working fluid, and the effects of different Newtonian viscosities and other fluid properties on flow pattern transition were not evaluated.

Since many industrial applications employ fluids with various viscosity values, it is still necessary to develop flow pattern maps considering the effects of the viscosity on the transition between each pattern.

Figure 3 illustrates a flow pattern map, simplified from Doron and Barnea (1996), which allows one to predict the flow pattern by measuring the average mixture velocity

[1] Each flow pattern, its characteristics and nomenclatures are described in Chapter 2.

(u_m) and solids concentration (C_s). Other operational variables may also be employed to predict the flow pattern.

Figure 3 – Flow pattern map illustration.

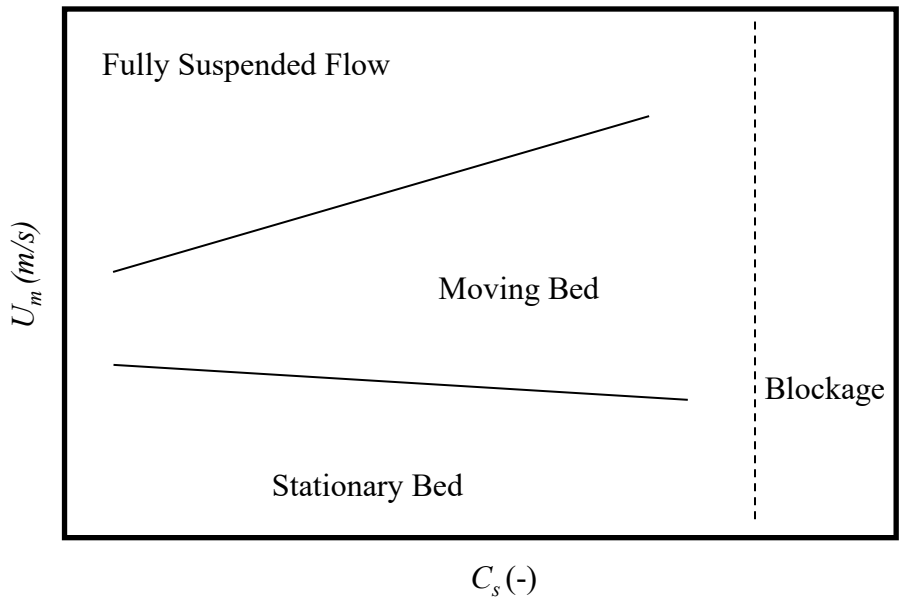

(Source: adapted from Doron and Barnea (1996))

1.3. Objectives

The objective of the present work is a liquid-solid flow pattern map development. The flow pattern map must account the effects of fluid viscosity on the flow pattern transition. The flow pattern map will be represented by the pressure drop per unitary length as a function of the fluid viscosity (μ) and Reynolds number (Re). It was also intended to determine the Euler number as a function of the Reynolds number and the fluid viscosity.

The fluid viscosity effects on the flow pattern transition were evaluated experimentally in a horizontal plexiglass test section. Three different Newtonian fluids were used on the tests. At first, water ($\mu = 10^{-3}$ Pa.s) [2] was employed to carry the solid particles, aiming to establish a reference. Then, two water-glycerin mixtures were

[2] μ is the fluid viscosity at constant pressure and temperature.

employed in order to vary the viscosity ($\mu = 3 \times 10^{-3}$ Pa.s and $\mu = 1.25 \times 10^{-2}$ Pa.s) of the working fluid, and the results were compared with those collected for water. Non-spherical Urea particles with an average size of $d_p = 1.44$ mm and density $\rho_p = 1480$ kg/m³ were used as the solid elements.

The pressure drop and the mixture mean velocity were measured for each experimental point, detailed in Chapter 3. Meanwhile, images of the transparent test section were captured. Flow pattern maps were developed with the collected data, representing the flow pattern to which the flow is submitted for a specific condition.

1.4. Document Structure

The present work is divided into five chapters: introduction, theoretical background and literature review, materials and methods, results, and final considerations.

The study is contextualized, and the problem is described in the first chapter, where the general objectives are defined.

The second chapter defines the fundamental concepts necessary for the comprehension of the present work. The chapter also presents the literature review, where previous works are discussed to establish the essential concepts and justify the present work's relevance.

The experimental apparatus and methodology are described in chapter three. The conditions in which each experiment was carried out, the equipment employed, and data treatment are discussed in the third section.

The experimental facility validation, as well as the results, are presented in the fourth chapter. Also, a discussion of the results and their implications are developed in the section.

Finally, the final considerations and conclusions are reported in chapter five.

2. THEORETICAL BACKGROUND AND LITERATURE REVIEW

This chapter introduces basic concepts essential for the comprehension of the present study. The most important topics addressed by the works found in the literature review are also discussed. The chapter aims to define the basic configurations and flow patterns detected in slurry flows and the essential physical principles involved in two-phase liquid-solid flows.

The pressure drop estimative and flow pattern prediction for biphasic solid-liquid flows are major industrial concerns, aiming to prevent catastrophic events due to pipeline blockage. The literature establishes that the pressure loss determination for biphasic settling flow is different from the monophasic (Kelessidis and Bandelis, 2005; Peker and Helvaci, 2011). Therefore, this chapter will first define the basic concepts of the pressure drop for monophasic flows. Then, the basic concepts of liquid-solid flow patterns will be introduced, and, finally, the literature review will be discussed.

2.1. Pressure loss on monophasic flows

2.1.1. Turbulence

The turbulence regime is vital for the study of viscous internal flows. The regime characterization is understood from the balance equations for the continuous phase. The fluid displacement is generally represented by the combination of the mass and momentum balance equations shown, respectively, in Equations (1) and (2) (Davidson, 2015; Peker and Helvaci, 2011). $\mathbf{u}_f$ is the fluid velocity, ρ_f is the fluid density, $\nabla \mathbf{g}\boldsymbol{\tau}$ is the stress tensor divergent, ∇p is the pressure gradient and $\frac{D()}{Dt}$ is the material derivative.

$$\frac{\partial \rho_f}{\partial t} = -\nabla \mathbf{g}\left(\rho_f \mathbf{u}_f\right) \quad \textbf{(1)}$$

$$\frac{D(\rho_f \mathbf{u}_f)}{Dt} = \nabla \mathbf{g}\boldsymbol{\tau} - \nabla p + \mathbf{F}_B \quad \textbf{(2)}$$

The momentum equation presents nonlinear terms, leading to complex and unpredictable solutions (Davidson, 2015), characterizing the flow turbulence.

Fluid flows are commonly divided into two flow regimes: laminar and turbulent (Davidson, 2015; White, 1976)[3]. Laminar flows are well behaved, and the fluid is displaced in parallel layers. In this condition, the momentum equation's nonlinear terms are relatively weak (Davidson, 2015). As the nonlinear terms become prevalent, the complexity and unpredictability of the flow increase (Davidson, 2015), leading to a turbulent flow due to random fluctuations in the three-dimensional velocity field (White, 1976).

The flow regime is defined through the Reynolds number, shown in Equation (3), as a function of the pipeline diameter d, fluid density ρ_f, velocity u_f and viscosity μ_f. The dimensionless parameter represents the ratio between inertial and viscous effects.

$$\mathrm{Re} = \frac{\rho_f u_f D}{\mu_f} \tag{3}$$

For internal flows, the regime's transition follows the criteria shown in Equation (4) (White, 1976).

$$\begin{cases} \mathrm{Re} < 2300 & \rightarrow \quad \text{Laminar Flow} \\ \mathrm{Re} \geq 2300 & \rightarrow \quad \text{Turbulent Flow} \end{cases} \tag{4}$$

2.1.1. Pressure loss for internal viscous flow

Internal flows are subjected to energy losses, resulting in pressure losses, also known as head losses. The mathematical formulation for monophasic pressure loss is based on a mechanical energy balance. Equation (5) represents the commonly employed expression for the estimative, which is deducted from the Bernoulli equation (Panton, 2013).

$$\Delta p = f \frac{L}{D} \frac{\rho_f}{2} u_f^{\,2} \tag{5}$$

[3] Although two flow regimes were quoted, some authors consider a transition region from laminar to turbulent.

In Equation (5), f is the friction factor, D is the pipeline internal diameter, ρ is the fluid density and u_f represents the mean fluid velocity (Panton, 2013).

The major losses represent the energy loss due to viscous friction inside the pipeline. The friction may occur between the fluid layers or between the fluid and the pipeline wall. Major losses are determined through the friction factor estimative. For laminar flow, the friction factor is determined by Equation (6).

$$f = \frac{64}{\mathrm{Re}} \tag{6}$$

Colebrook's (1939) correlation, shown in Equation (7), is often employed for turbulent friction factor determination. The friction factor is determined as a function of the pipeline wall roughness ratio e/D and the Reynolds number.

$$\frac{1}{\sqrt{f}} = -2.0 \log\left(\frac{e/D}{3.7} + \frac{2.51}{\mathrm{Re}\sqrt{f}}\right) \tag{7}$$

However, Colebrook's (1939) correlation requires an iterative solution since it is impossible to solve the equation for the friction factor (f) analytically. The Blasius friction factor, expressed in Equation (8), does not require the iterative solution and yet, provides a good estimative for the friction factor, as long the restriction of $\mathrm{Re} < 10^5$ is respected (Fox et al., 2009; Pope, 2000; White, 2010).

$$f = \frac{0.316}{\mathrm{Re}^{0.25}} \tag{8}$$

The minor losses represent the energy loss due to specific components in the pipeline, such as area reduction or expansion devices, and they are estimated through Equation (9). The constant K is determined for each device on the system and is provided by the manufacturer. Then, the minor loss is determined by the sum of the pressure loss caused by each component.

$$\Delta p = K \frac{\rho u_f^{\,2}}{2} \qquad \textbf{(9)}$$

2.2. Flow Patterns

Slurry flows are defined by Capecelatro and Desjardins (2013) as liquid-solid flows containing settling particles in a carrier fluid, in which the solids are considered to be a dispersed phase and the liquid a continuous phase (Capecelatro and Desjardins, 2013; Peker and Helvaci, 2011). The continuum approach assumes that a media composed of several particles behaves as an artificial continuous, disregarding local behavior and the effects of individual particles (Kloss et al., 2009). The discrete phase analysis evaluates each individual particle motion (Peker and Helvaci, 2011).

Due to the particle's settling tendency, different flow patterns may occur in slurry flows, depending on the combination of solids concentration, slurry flow rate, pipeline inclination, among other parameters (Kelessidis and Bandelis, 2005). The present section aims to classify and describe those flow patterns.

Several nomenclatures and divisions were used in the literature to characterize the different flow patterns in a pipe. In that sense, it is important to mention that in the present study, the flow pattern characterization established by Doron and Barnea (1996) was employed, dividing the flow patterns as fully suspended flow, flow with a moving bed and flow with a stationary bed.

All solid particles' suspension characterizes the fully suspended flow (Figure 4.a), occurring at high slurry flow rates (Doron and Barnea, 1996). This flow pattern is subdivided into two subcategories, the pseudo homogeneous suspension, in which all particles are uniformly suspended, and the heterogeneous suspension flow, consisting of the formation of a non-uniform particle concentration profile in the cross-section of the pipe (Doron and Barnea, 1996; Peker and Helvaci, 2011).

When a moving packed layer is formed at the bottom of the pipe, due to particle settling at lower flow rates, the flow is characterized as flow with a moving bed (Figure

4.b). Then, the upper layer is filled with a heterogeneous suspension flow (Doron and Barnea, 1996).

When the slurry flow rate is too low to move all particles accumulated at the bottom of the pipe, a flow with a stationary bed (Figure 4.c) is observed, composed of three layers: a stationary layer at the bottom of the pipe, a moving bed on top of the stationary layer and the rest of the pipe is filled with a heterogeneous suspension flow (Doron and Barnea, 1996; Peker and Helvaci, 2011).

Figure 4 – Doron and Barnea's (1993) classification on flow patterns: a) fully suspended flow, b) flow with a moving bed, and c) flow with a stationary bed.

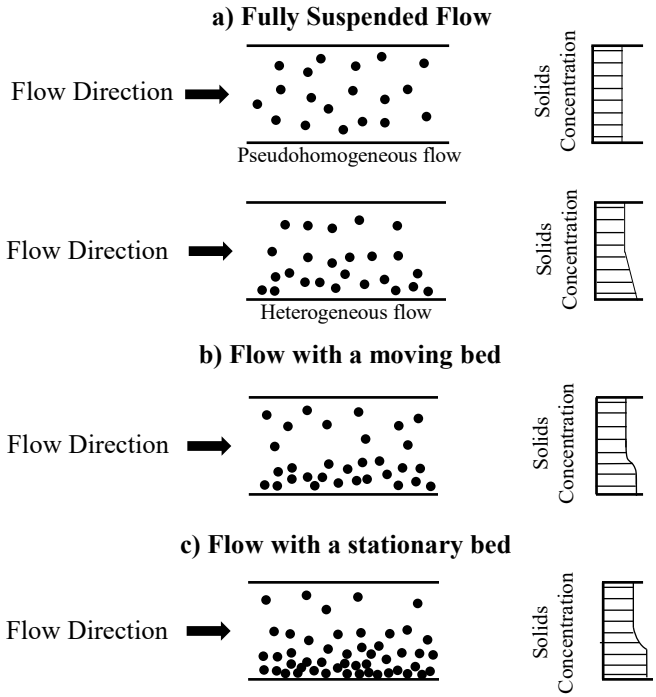

(Source: Adapted from Peker and Helvaci (2011)).

2.3. Review on Flow Patterns

A literature review of flow patterns is presented in this section, discussing the relevant parameters on the flow pattern study and the most important correlations proposed for the biphasic liquid-solid pressure drop and friction factor determination.

The liquid-solid flow patterns described in Section 2.2 were initially referred to as flow regimes by Durand (1953, *apud* Doron et al., 1987) and divided into simpler categories. As new studies were developed, different authors employed new characterizations, resulting in a great variety of definitions (Doron et al., 1987). Table 1 shows the classification used in previous works for each pattern and the equivalent nomenclature employed in the current work, according to the definition shown in Section 2.2. The first column of the table represents the authors' flow pattern nomenclatures. The equivalent terminology defined in this work is presented in the right column. Analog terminologies in the literature and in the present work are characterized by the equivalent letters.

Table 1 – Flow patterns divisions and nomenclature convention for the present work.

Nomenclature in the literature	Authors	Nomenclature in the present work
a) Non-deposit flow regime b) Deposit flow regime	Durand (1953) Condolios and Chapus(1963)	a) Fully suspended flow b) Flow with a moving bed/flow with a stationary bed
a) Homogeneous flow b) Heterogeneous suspension flow c) Saltation flow d) Bedload	Faddick (1970)	a) Fully suspended flow b) Fully suspended flow c) Flow with a moving bed d) Flow with a stationary bed
a) Homogeneous flow b) Heterogeneous flow c) Saltation flow d) Stationary bed	Turian and Yuan (1977)	a) Fully suspended flow b) Fully suspended flow c) Flow with a moving bed d) Flow with a stationary bed
a) Homogeneous flow b) Heterogeneous flow c) Heterogeneous and sliding-bed flow d) Saltation and stationary flow	Parzonka *et al.* (1981) Shamlou (1987)	a) Fully suspended flow b) Fully suspended flow c) Flow with a moving bed d) Flow with a stationary bed

a) Fully segregated flow regime b) Heterogeneous flow regime	Brown (1991)	a) Flow with a moving bed/flow with a stationary bed. b) Fully suspended flow

(Source: author)

The detection of liquid-solid flow patterns is based mainly on visual data (Doron et al., 1987; Doron and Barnea, 1996; Kelessidis and Bandelis, 2005). However, most authors only defined each flow pattern. However, they did not describe the criteria experimentally employed to detect each of them, resulting in a subjective factor in identifying the flow patterns, which may be significantly intensified in transition regions.

For slurry flows, the relationship between the pressure drop and the mixture mean velocity is significantly different from that of a pure liquid flow (Doron et al., 1987; Peker and Helvaci, 2011). The pressure drop in a slurry flow is generally higher than that of the monophasic flow, for a fixed mean velocity value, due to the area reduction effect of the particles, especially for low mixture velocities, in which a bed of particles is formed at the bottom layer of the pipeline (Kelessidis and Bandelis, 2005). Thus, several authors proposed correlations and formulations to predict the pressure drop in a slurry flow.

Durand (1953, *apud* Doron et al., 1987) first determined an empirical correlation for predicting the pressure loss of slurry flows in a pipe. The correlation depends on the particles and the pipe's geometric factors, on the solids concentration, on the fluid and the particles' properties, on flow characteristics, and the value of the pressure drop for the monophasic flow. Newitt et al. (1955, *apud* Gillies et al., 1991) proposed three empiric correlations, depending on the slurry mean velocity and, consequently, on the flow pattern. The correlation depended on similar parameters to that of Durand (1953, *apud* Doron et al., 1987), and each correlation was employed to a specific flow pattern. Faddick (1970) evaluated Durand's (1953) pressure drop correlation for a woodchip-water mixture. The author found out that the correlation was not accurate for all cases studied since the scale factor, determined by the ratio between particle and pipe diameter, is not considered. According to the author, a shape factor should also be considered, especially for *plate-shaped* particles, since the effects of particle shape are as significant as the particle size.

The most significant experimental database was obtained by Turian and Yuan (1977), in which 2848 points were collected to develop a correlation for the slurry pressure loss through the determination of the friction factor. The correlation shows the friction factor's dependence on the volumetric concentration, drag coefficient, slurry mean velocity, solid-liquid density ratio, and a reference friction factor for pure liquid flow. The model contains five constants, which are fitted according to the flow patterns studied, shown in Table 1.

A physical model was proposed by Doron et al. (1987) to predict the pressure loss for slurry flows and the velocities in which the transition of flow patterns is detected. The model consisted of dividing the problem into two layers, in which the bottom and upper layer represented, respectively, the bed of particles and the heterogeneous flow, as shown in Figure 5a. However, the model was inaccurate for predicting the stationary bed. In several cases where a stationary bed was observed experimentally, the model indicated flow with a moving bed (Doron and Barnea, 1993). Therefore, Doron and Barnea (1993) successfully developed a three-layer model, in which the upper, middle and bottom layers represented, respectively, a heterogeneous flow, a moving bed and a stationary bed, as shown in Figure 5b. The prediction of the flow patterns was based on the assumption that a minimal velocity is required to induce the bed movement. The determination of the limiting value for the velocity was based on a torque balance on a particle at the interface between the layers. The results obtained with the model were compared with experimental data collected for several operational conditions, and it was concluded that there was a significant improvement from the results of the two-layer model. However, the experimental facility employed did not have a controlling system for the particle concentration. Therefore, the delivered particle concentration (particle concentration in the inlet of the test section) changes over time and with the flow rate, which may not represent properly industrial processes.

Finally, Doron and Barnea (1996) employed the three-layer model and collected experimental data to develop flow pattern maps, presenting the effects of particle diameter and density, solids concentration, pipe diameter, and volumetric flow rate on the transition from one pattern to another. The maps are shown as a function of the mixture mean velocity and solids concentration. However, the applicability of each map is restrained to the viscosity of the fluid employed.

Figure 5 – Representation of (a) Doron et al. (1987) two-layer model and (b) Doron and Barnea (1993) three-layer model.

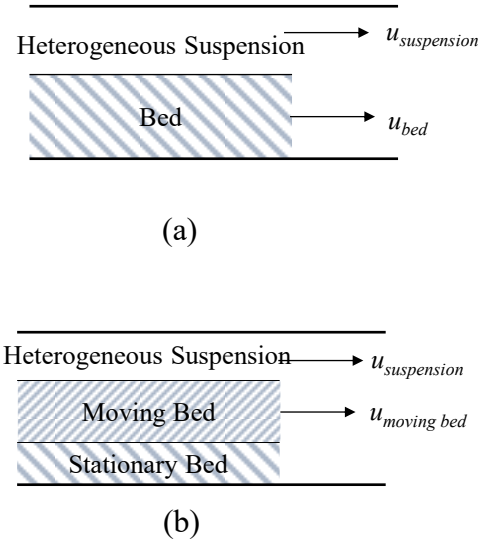

(Source: Adapted from (a) Doron et al. (1987) and (b) Doron and Barnea (1993))

Another two-layer model was proposed by Gillies et al. (1985) and improved in Gillies et al. (1991). The first version of the model could not account for small particles with 74μm or smaller. The model was later improved to consider smaller particles.

The most important models for pressure drop and friction factor prediction for slurry flow in pipes found in the literature are summarized in Table 2. In this table, s is the solid-to-liquid density ratio, u_m is the slurry (or mixture) mean velocity (also known as bulk velocity), ε_s is solids volumetric concentration of the slurry, D is the pipe diameter, f is the friction factor, Δp is the slurry pressure drop, Δp_{mono} is the pressure drop for the carrier fluid monophasic flow, C_D is the drag coefficient, V_p is the particle terminal settling velocity, g is the acceleration due to gravity, t is the shear stress, P is the perimeter, A_b is the bed cross-section area and A is the cross-section area above the bed. Other variables specific to each model are discussed in the table.

Table 2 – Correlations for pressure drop determination on liquid-solid biphasic flows.

Authors	Model	Obs.
Durand (1953)	a) $\Phi = \frac{\Delta p - \Delta p_{mono}}{\varepsilon_s \Delta p_{mono}} = K\left[\frac{u_m{}^2\sqrt{C_D}}{gD(s-1)}\right]^{-n}$	Constants K and n are experimentally adjusted.
Newitt et al. (1955)	a) $\Phi = 0.6(s-1)$ b) $\Phi = 1100\frac{gDV_p}{u_m{}^3}(s-1)$ c) $\Phi = 66\frac{gD}{u_m{}^2}(s-1)$	Models are employed according to the flow pattern: a) Pseudohomogeneous flow b) Heterogeneous flow c) Flow With a moving Bed
Turian and Yuan (1977)	a) $f_m - f_f = K_1 C_*{}^{K_2} f_f{}^{K_3} C_D{}^{K_4}\left[\frac{u_m}{gD(s-1)}\right]^{K_5}$	The constants K_n are experimentally determined, according to the flow pattern. The sub-indexes s and f refers, respectively, to the solid and fluid phase.
Doron et al. (1987)	a) $A_h\frac{dP}{dx} = -\tau_h P_h - \tau_l P_l$ b) $A_b\frac{dP}{dx} = -F_{bd} - \tau_b P_b + \tau_l P_l$	Pressure drop for the: a) Upper layer, according to Figure 5a b) Bottom Layer, according to Figure 5a P represents the perimeter for each phase (heterogeneous suspended and settled bed phases).
Doron and Barnea (1993)	a) $A_h\frac{dP}{dx} = -\tau_h P_h - \tau_{hmb} P_{hmb}$	The sub-index h refers to the upper layer and hmb to the interface between the heterogeneous suspended flow and the moving bed layer.

(Source: author)

In previous works, it was well stated that slurry means velocity, liquid to solid density ratio, pipe and particle diameter, drag coefficient, and solids concentration are relevant factors for the flow pattern prediction in horizontal pipelines. However, the influence of the dynamic viscosity is not explicitly considered.

The behavior of slurries in annular spaces was not studied until Kelessidis and Bandelis (2005) developed their work. According to the authors, the flow pattern qualitative behavior in annular spaces are similar to those in pipes, however, the velocity in which each flow pattern is formed, changes. Regarding eccentric annuli, higher flow rates are required to achieve flow patterns. The authors also evaluated three different fluids as the carrier fluid: the water and two different carboxymethylcellulose[4]-water mixtures. The water and one of the CMC-water mixtures presented Newtonian behavior, while the other CMC-water fluid was characterized as a power-law non-Newtonian fluid. The work emphasized the relevance of the fluid viscosity on bed erosion, dividing the phenomena into two leading causes: i) impact erosion and ii) shearing erosion. The first one is defined as the bed erosion caused by the fluid's impact on the particle's full exposed area and prevailed for lower viscosity fluids. On the other hand, the shear erosion was associated with higher viscosity fluids, where the particle transport happens due to fluid shearing.

Although Kelessidis and Bandelis (2005) provided interesting information regarding the influence of the viscosity on the bed erosion process, a correlation and a flow pattern map evaluating the effects of μ on the transition between the different flow patterns is still necessary.

2.4. Parameters Affecting Cuttings Transport

For this section, the objective was to find in the literature the relevant parameters regarding cuttings transport in drilling operations, whose effect on flow pattern transition was not studied yet.

The complexity of the liquid-solid flow in drilling operations can be associated with the high number of parameters that affect cuttings removal. Nazari et al. (2010) evaluated the influence of several parameters in solids transport, comparing to how easily this parameter is controlled on field conditions. A sensitivity analysis was employed to determine each operational variable's relevance in the cuttings transport problem. The

[4] Carboximetilcellulose – CMC.

variables which the authors studied, its influence on the hole cleaning efficiency, and other authors, which also studied each one of them, are show in Table 3.

Table 3 – Nazari et al. (2010) studied parameters and conclusion on their influence over cuttings transport.

Parameter	Influence on Hole Cleaning Efficiency	Authors
Volumetric Flow Rate	High	Hopkin (1967) Hussaini and Azar (1983) Larsen et al. (1997)
Rheological Properties	Moderate	Larsen et al. (1997)
Wellbore Angle	High	Hussaini and Azar (1983) Locket et al. (1993)
Fluid Density	Low	Hopkin (1967) Hussaini and Azar (1983) Larsen et al. (1997)
String Rotation	High	Williams and Bruce (1951) Hopkin (1967) Locket et al. (1993) Hemphill and Ravi (2006) Han et al. (2009) Akhshik et al. (2015) Hashemabadi and Ghasemikafrudi (2016) Sayindla et al. (2017)
Hole Eccentricity	High	Martins et al. (1996) Walker and Li (2000) Hemphill and Ravi (2006) Ghasemikafrudi and Hashemabadi (2016) Dewangan and Sinha (2016)
Cuttings Size	Low	Larsen et al. (1997) Walker and Li (2000) Ghasemikafrudi and Hashemabadi (2016)

(Source: adapted from Nazari et. al (2010))

As shown in Table 3, the volumetric flow rate plays a very relevant role in cuttings transport, especially since it can be controlled in the field (Nazari et al., 2010). This behavior is associated with a higher drag force provided by the fluid to lift and carry the particles.

The effects of the volumetric flow rate in cuttings transport were studied by Williams and Bruce (1951), where the annular flow velocity was associated with the capacity of maintaining the borehole clean. This association can also be found in Hopkin's (1967) work, where the effects of hole enlargement on solids removal were studied. The author characterized the parameter as a velocity reduction element, responsible for a decrease in cuttings removal. Both studies also established the importance of fluid properties in the particle transport problem. The properties mentioned were fluid viscosity and density, which align with the parameters shown in Table 3.

Although the importance of fluid velocity and properties in the cuttings removal problem was well established, Hussaini and Azar (1983) suggested that each parameter's effects depended on the wellbore inclination. According to the authors, increasing the fluid velocity is more relevant for vertical wellbores, while fluid properties, such as the viscosity and density, increased particle removal for horizontal and low angled wellbores. A similar conclusion was presented by Larsen et al. (1997): lower viscosity muds performed better for high angled wells due to the higher velocity achieved.

The behavior observed by Hussaini and Azar (1983) and Larsen et al. (1997) is associated with the drag force F_D, provided by the fluid velocity u_f. For vertical wellbores the drag force opposes the particle weight F_w, as illustrated in Figure 6a. On the other hand, for low inclined wellbores, only the vertical component of the drag force $F_{D\,y}$ counteracts the particle weight, as shown in Figure 6b. From this perspective, fluid properties should only be responsible for reducing particle settling until they are removed.

Figure 6 - Effects of fluid velocity counteracting particle weight in a (a) vertical well and a (b) low inclined well.

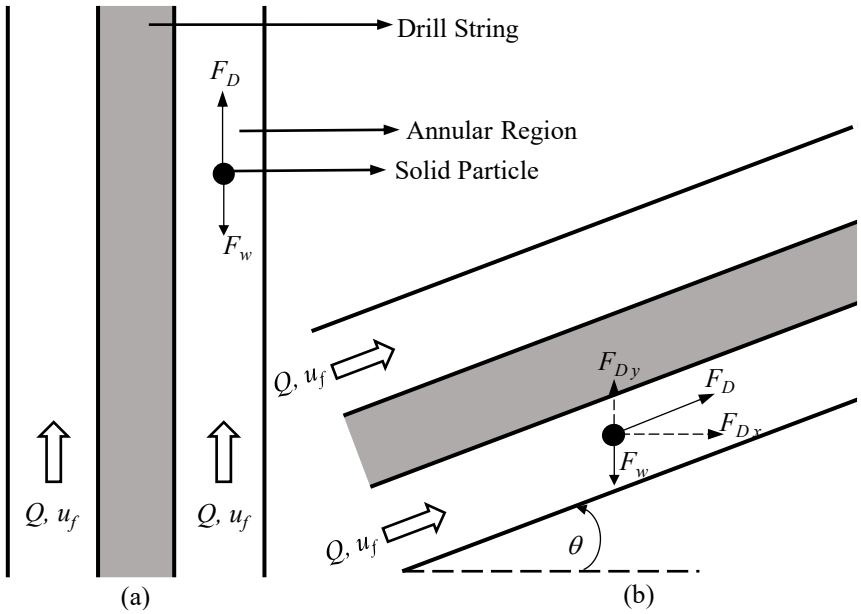

(Source: author)

Locket et al. (1993) affirmed that particle settling is decreased by the presence of turbulence in the flow due to the sudden changes in the fluid path, which is supported by Doron and Barnea (1987) and Williams and Bruce (1951). Similarly, Ghasemikafrudi and Hashemabadi (2016) defended that higher fluid velocity improves cuttings transport. However, employing higher density fluids enables the same cutting carrying capacity at lower flow rates.

Regarding the effects of rotation in the drill string, Williams and Bruce (1951) first emphasized the benefits of drill string rotation in cuttings removal, which was most pronounced in high viscosity muds. Locket et al. (1993) experimentally evaluated rotation effects in solids transport for different wellbore angles, observing a significant improvement in particle transport with the presence of rotation, independent of the wellbore angle. Hemphill and Ravi (2006) extended their work and evaluated the effects of drill string rotation in cuttings removal and pressure drop. The pressure drop increased as the rotation increased, especially for high eccentric wellbores, supported by Ghasemikafrudi and Hashemabadi (2016) and Sayindla (2017). The authors also concluded that rotation is especially beneficial for eccentric wellbores, in which only axial flow is not enough to transport the particles along with the annular space.

It was well established that rotation is beneficial for cuttings removal. However, Han et al. (2009) concluded that this effect is more pronounced at lower mixture velocities and almost negligible at higher flow rates, supported by Akhshik et al. (2015). Ghasemikafrudi and Hashemabadi (2016) explained the benefits of cuttings removal due to the drill string rotation: it provides a circular component to the flow, which results in a helicoidal flow, enhancing the capacity to carry the cuttings near to the wall, a region where poor hole cleaning occurs more frequently.

2.5. Chapter Synthesis

It was verified that the fluid dynamics viscosity is accounted for among the most relevant parameters in cuttings transport. However, there is a lack of flow pattern predicting tools that explicitly considered its influence, allowing one to predict the pressure drop and flow pattern transition for Newtonian fluids different from the water.

The present study was developed in a horizontal pipeline due to the conclusion of the dynamic viscosity relevance on cuttings transport at low angled wellbores. Volumetric flow rate and pressure drop were established as the reference parameters in the flow pattern map development.

The following specific objectives were proposed for the present work:

a) Dimensional analysis development for a liquid-solid flow in a horizontal pipeline. The resulting dimensionless groups should give information about physical aspects of the biphasic liquid-solid flow. Besides that, the non-dimensional expression of the results may expand the scope of the results.
b) Design of the experimental apparatus for the liquid-solid biphasic flow. Also, the development of the experimental methodology for the flow pattern map development.
c) Assembly and commissioning of the experimental apparatus.
d) Validation of the measuring devices.
e) Development of flow pattern maps as a function of the pressure drop, dynamic viscosity, and Reynolds number.

The equipment and methodology employed are described in Chapter 3.

3. MATERIALS AND METHODS

The materials, equipment, and methodology employed for the thesis development are described in this chapter. For the evaluation offluid viscosity effects in the transition between the flow patterns, an experimental apparatus was designed, and a methodology was developed.

The chapter was divided according to the steps followed for the work development:

- Step 1: Dimensional analysis.
- Step 2: Experimental apparatus design.
- Step 3: Experimental methodology.
- Step 4: Experimental apparatus assembly.

3.1. Step 1 – Dimensional Analysis

The dimensional analysis was the first step in the apparatus design and methodology development, aiming to reduce the experiment's parameters. Also, the procedure allowed raising the most relevant dimensionless groups and physical effects affecting the experiment. Besides, flow pattern maps will be expressed in terms of the dimensionless groups and compared to data obtained in the dimensional form, which may increase the scope of the results.

3.1.1. Application of Buckingham π-theorem for a slurry flow

The first step to applying the Buckingham π-theorem consists of determining the most relevant variables for the problem and defining a characteristic function (Panton, 2013; White, 2010; Yarin, 2012). The experiment consists of a liquid-solid flow in a horizontal pipeline in which it is assumed that the working fluid behaves as an incompressible Newtonian fluid in isothermal conditions. Although the particles employed in the experimental tests are not spherical, they are assumed to be spherical with a constant average diameter for the dimensional analysis.

Based on the dimensional analysis developed by Faddick (1970), the dependent variable is assumed to be the pressure drop in the test section. In agreement with data shown in Chapter 2, the pressure drop for an internal liquid-solid flow is a function of the

mixture mean velocity u_m, particle delivered concentration C_s, diameter d_p and density ρ_p, fluid viscosity μ and density ρ_f, acceleration due to gravity $\boldsymbol{g}$ and hydraulic diameter D_h, which is equivalent to the pipeline diameter D for the present study. The variables which affect the slurry pressure drop in the pipeline are illustrated in Figure 7.

Figure 7 - Parameters affecting the pressure drop in slurry flow.

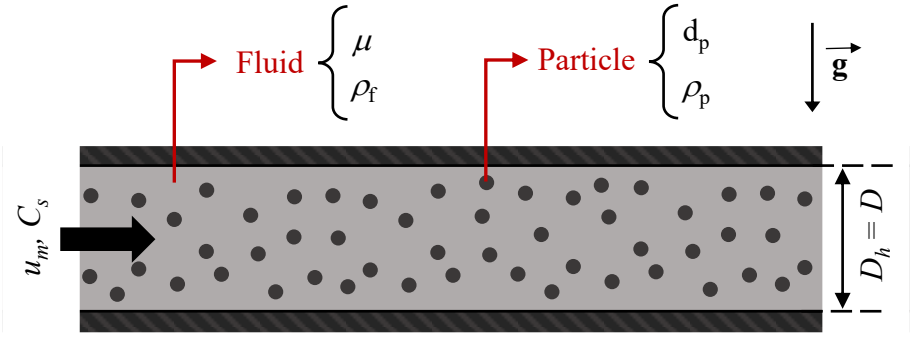

(Source: author).

Based on the parameters shown above, the characteristic function for the pressure drop may be written as follows:

$$\Delta p = \beta(u_m, \mu, \rho_f, \rho_p, d_p, D, C_s, g) \quad \textbf{(10)}$$

According to the theorem, a problem described by n dimensional variables is represented by $k = n - j$ dimensionless parameters (Panton, 2013; White, 2010), where j is the rank of the dimensional matrix.

The dimensional matrix, shown in Table 4, represents the dimensional parameters in terms of the basic dimensions {MLT}[5], presenting the exponents of each basic dimension for all n dimensional parameters (Panton, 2013).

[5] The dimensions M L T refer, respectively, to mass, length and time.

Table 4 – Dimensional matrix developed for the dimensional analysis procedure, presenting the exponents of each basic dimension for each variable.

	Δp	u_m	μ	ρ_f	ρ_p	d_p	D	C_s	g
M	1	0	1	1	1	0	0	0	0
L	-1	1	-1	-3	-3	1	1	0	1
T	-2	-1	-1	0	0	0	0	0	-2

(Source: author)

The evaluation of the determinant of all possible square submatrices, composed of all combinations of the dimensional parameters, allows one to determine the rank of the dimensional matrix, j (Panton, 2013). According to Panton (2013), the dimensional matrix's rank is equivalent to the size of the largest square submatrix with a nonzero determinant. For the dimensional matrix given in Table 4, a rank $j = 3$ was found.

A set of j recurrence parameters must be determined to find the dimensionless π groups (Panton, 2013). The set of variables must be linearly independent; that is, the determinant of the matrix constituted by the repeating variables must result in a nonzero value.

Faddick (1970) applied the Buckingham π theorem for a slurry flow in a pipe, and the recurrence parameters u_m, ρ_f and D_h were chosen. The same repeating variables were selected for the present work, consistent with the linear independence criteria. Similarly, Glicksman (1994) developed the theorem for a gas-solid fluidized bed, and the equivalent parameters were employed.

Six π groups were found employing the theorem with the procedure described. The dimensionless groups and previous works in which similar parameters were found are shown in Table 5.

Table 5 – Relation of the π groups determined in the present study and works in which similar groups were presented.

Pi groups determined in the present work		Previous works in which similar groups were determined
$\Pi_1 = \frac{\Delta p}{\rho_f u_m^{\ 2}} = Eu$	(11)	Faddick (1970) Glicksman et al. (1994)
$\Pi_2 = \frac{\rho_f u_m D}{\mu} = \mathrm{Re}$	(12)	Faddick (1970) Glicksman et al. (1994) Martins et al. (1996) Duan et al. (2008) Cao et al. (2009)
$\Pi_3 = \frac{gd}{u_m^{\ 2}} = Fr^{-1}$	(13)	Faddick (1970) Glicksman (1984) Glicksman et al. (1994) Cheng and Zhu (2008b) Natarajan et al. (2014)
$\Pi_4 = C_s$	(14)	Faddick (1970) Glicksman (Glicksman, 1984) Glicksman et al. (1994) Cheng and Zhu (2008b) Natarajan et al. (2014)
$\Pi_5 = \frac{\rho_p}{\rho_f}$	(15)	Faddick (1970) Glicksman (Glicksman, 1984) Glicksman et al. (1994) Martins et al. (1996) Cheng and Zhu (2008b) Cao et al. (2009)
$\Pi_6 = \frac{d_p}{D}$	(16)	Faddick (1970) Glicksman (Glicksman, 1984) Glicksman et al. (1994) Martins et al. (1996) Cheng and Zhu (2008b)

(Source: author)

The reduced form of the characteristic function is expressed in terms of the π groups presented in the Table 5 and is shown in Equation (17).

$$Eu = \frac{\Delta p}{\rho_f u_m{}^2} = \phi\left(\frac{\rho_f u_m D}{\mu}, \frac{gD}{u_m{}^2}, C_s, \frac{\rho_p}{\rho_f}, \frac{d_p}{D} \right) \tag{17}$$

The problem, which initially consisted of $n = 9$ dimensional variables, is now described by $k = n - j = 6$ dimensionless parameters, which are discussed individually below.

The non-dimensional pressure drop, normalized by the dynamic pressure, is presented in Equation (11) and is a function of the other π groups. The parameter is also known as the Euler number, which characterizes the energy losses due to friction in a confined flow. A similar parameter is also presented in the dimensional analysis developed by Glicksman et al. (1994) for a gas-solid flow and Faddick (1970) for a liquid-solid flow.

The ratio between inertial and viscous effects is represented by the Reynolds number, Equation (12), and is often found as a relevant parameter governing multiphasic flows, whether they are gas-solid (Cao et al., 2009; Glicksman et al., 1994) or liquid-solid (Duan et al., 2008; Faddick, 1970; Martins et al., 1996).

The relationship between inertial and field effects, described in the given problem by the gravity, is represented by Equation (13), which may be written as a form of Froude's number (Cheng and Zhu, 2008b; Glicksman, 1984; Natarajan et al., 2014). The Froude's number is described as the ratio of inertial to gravitational forces (Glicksman et al., 1994) and, according to Yeckel and Middleman (1987), is written as follows:

$$Fr = \frac{U_0{}^2}{g l_0} \tag{18}$$

in Yeckel and Middleman (1987), the dimensionless group is written as a function of the gas-liquid mean velocity U_o and a characteristic length l_0.

Since the solids concentration is already a dimensionless parameter, Equation (14) is the variable itself (Faddick, 1970). Dimensionless groups equivalent to the concentration are often found in gas-solid flow studies representing particles' concentration in the flow given particle injection rate (Cheng and Zhu, 2008a; Glicksman et al., 1994; Natarajan et al., 2014). In the present work, the delivered concentration value will be kept constant over the tests, aiming to isolate the viscosity's effects.

The last two π groups, Equations (15) and (16), represented, respectively, the density ratio between the solids and liquid and the geometric scale factor between the particle and the hydraulic diameter. The particle and pipeline diameters will not be changed over the tests and the particle density. Also, the variation of the specific mass for the different fluids employed was assumed to be negligible. Therefore, these π groups are also considered constant over the experiments.

Considering that Π_3, Π_4, Π_5 and Π_6 are constant over the experiments, the reduced function now depends only on the Reynolds and Froude's number, as shown in Equation (19).

$$\frac{\Delta p}{\rho_f u_m{}^2} = \phi\left(\frac{\rho_f u_m D}{\mu_f}, \frac{gD}{u_m^2}\right) \tag{19}$$

3.2. Step 2 – Experimental apparatus design

The experimental apparatus's concept and design are introduced in the present section and the objective of each component employed. The test procedure's general concept consists of measuring the pressure drop on the pipeline while the volumetric flow rate is slowly increased so that the transition between flow patterns can be detected.

3.2.1. Flow loop concept and description

The experimental apparatus consists of a PVC pipeline with a total L = 8 m and internal diameter D = 36 mm. A 2 m long plexiglass test section is placed at the end of the horizontal section of the loop, as represented in Figure 8. The dimensions quoted are justified in Section 3.2.3.

The liquid-solid mixture is stored in the mixing tank (I) at room temperature and pumped by a positive displacement pump (II). The biphasic volumetric flow rate of the biphasic mixture, its temperature, and concentration are measured by a *Coriolis* flowmeter (III). The liquid-solid flow enters the test section (IV), in which the pressure drop is determined by a differential pressure transducer, represented in Figure 8 by Δp (1). The pressure drop in the whole system is measured at the Δp (2) transducer. Finally, the mixture leaves the test section and returns to the feeding system through valve (a).

Figure 8 – Experimental bench schematic.

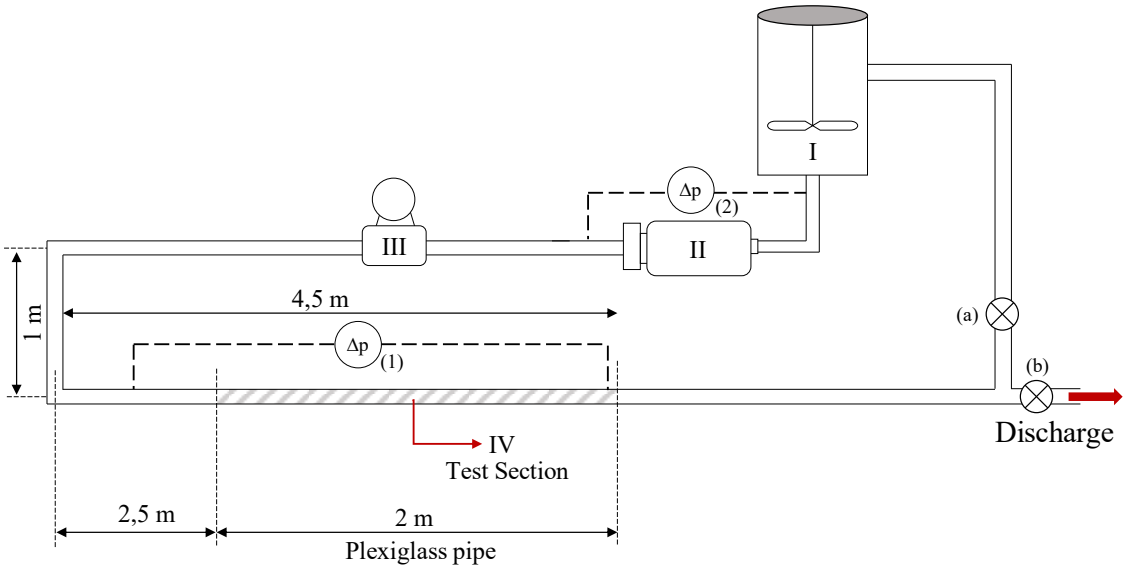

(Source: author)

During the experiments, valve (b) stays closed while the valves (a) is open. After the test, the particles are filtered and removed from the system. Then, valve (b) is opened, forcing the fluid flow to the discharge.

Since most of the flow pattern detection is performed by visualization, an *EOS Canon T2i Rebel* camera is positioned to capture the test section's images during the experiment. Also, a scale was positioned in the visualization window for further data treatment.

Data collected by the flow meter (III) feeds a control system, allowing one to determine the slurry Reynolds number by controlling the rotation of the helical pump (II)

with a frequency inverter[6]. The Reynolds number is defined in the test section diameter D and considers the slurry mean velocity, determined through the volumetric flow rate, as shown in Equation (20).

$$\mathrm{Re} = \frac{\rho_f u_m D}{\mu_f} = \frac{4}{\pi}\frac{\rho_f Q}{\mu_f D} \tag{20}$$

3.2.2. Control system

A routine was developed in the Labview software in order to treat and store the collected data. Also, the software was employed to control the volumetric flow rate in the experimental bench. The control facility designed for the experimental rig is illustrated in Figure 9 and is described below.

Figure 9 – Illustration of the equipment control in the experimental apparatus.

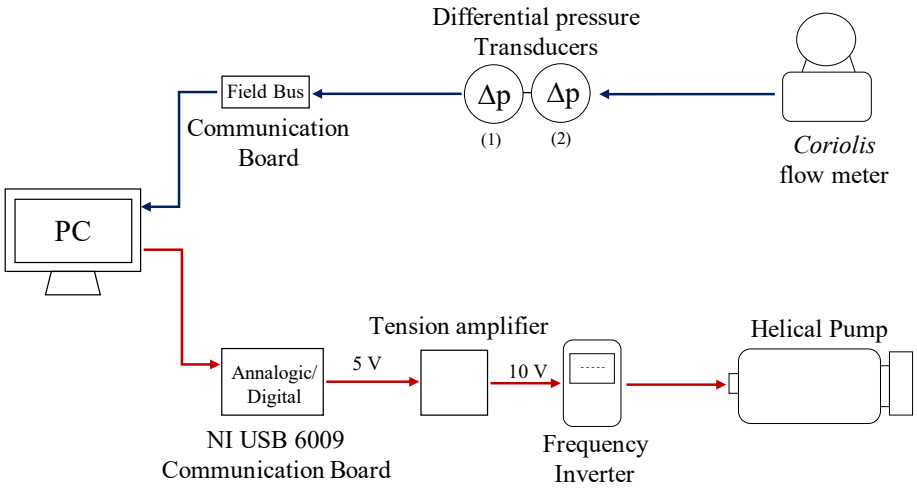

(Source: author).

In Figure 9, the blue lines represent the input signal provided by the measuring devices. The red line denotes the output signal for the volumetric flow rate control.

The interface between the measuring equipment and the computer was carried through a Fieldbus protocol, allowing the equipment to be connected in series, feeding

[6] The design of the control system is detailed in Section 3.2.2.

the routine with a digital signal. The signal will communicate with the computer through a Fieldbus communication board.

The helical pump must be controlled based on the values measured by the *Coriolis* flowmeter. Therefore, the Labview routine collected the data from the measurers and controlled the analogical components through a *National Instruments* NI USB 6009 analogic-digital communication board.

The combination of the analogic interface and the tension amplifier in series will provide a tension from 0 to 10 V, depending on the measured flow rate, which will feed a frequency inverter, responsible for controlling the pump rotation consequently, the volumetric flow rate.

The parameters measured by each instrument and the measuring characteristics are shown in Table 6.

Table 6 - List of instruments and parameters measured in the experimental rig.

Device	Measured Parameters	Standard Uncertainty
Coriolis mass flow meter	ρ – density [kg/m³] T – temperature [K] Q – volumetric flow rate [m³/s]	± 0.5%
Rosemount transducer	Δp – differential pressure [Pa]	± 0.41%
SMAR transducer	Δp – differential pressure [Pa]	± 0.4%

(Source: author)

3.2.3. Dimensions and Equipment Specification

A positive displacement pump was employed in order to pressurize the liquid-solid mixture, which was previously specified. For the pump specification, it was necessary to establish the experimental rig's dimensions, such as the internal pipeline diameter, length and the maximum mixture velocity. Kelessidis and Bandelis (2005) presented flow pattern maps, in which the velocity required for the water to suspend glass particles in an

annular section with hydraulic diameter d_h = 30 mm was around u_m = 1.6 m/s, serving as the base for the pump selection. To work with some security margin, a maximum value of u_{m_crit} = 4 m/s was assumed.

The selected pipeline has a commercial internal diameter of D = 36 mm. The given dimension choice was based on two main reasons: (i) the estimative for the pressure drop in the test section and (ii) the flow pattern formation.

The pressure drop estimated for commercial plexiglass pipelines with greater diameter was lower than the minimum span required by the pressure transducers available in the laboratory. Also, higher diameters required higher flow rates, which implied much more expensive helical pumps. The pressure drop was estimated for the water and the two water-glycerin mixtures employed in the present work. Three values of internal diameter [D = 26, 36, 49 mm] were considered based on the commercial plexiglass pipes available in the local sellers. The estimation is presented in Figure 10, considering the pressure transducer's maximum and minimum limits, and the calculation is detailed in Appendix A.

Figure 10 - Pressure drop estimative in the test section

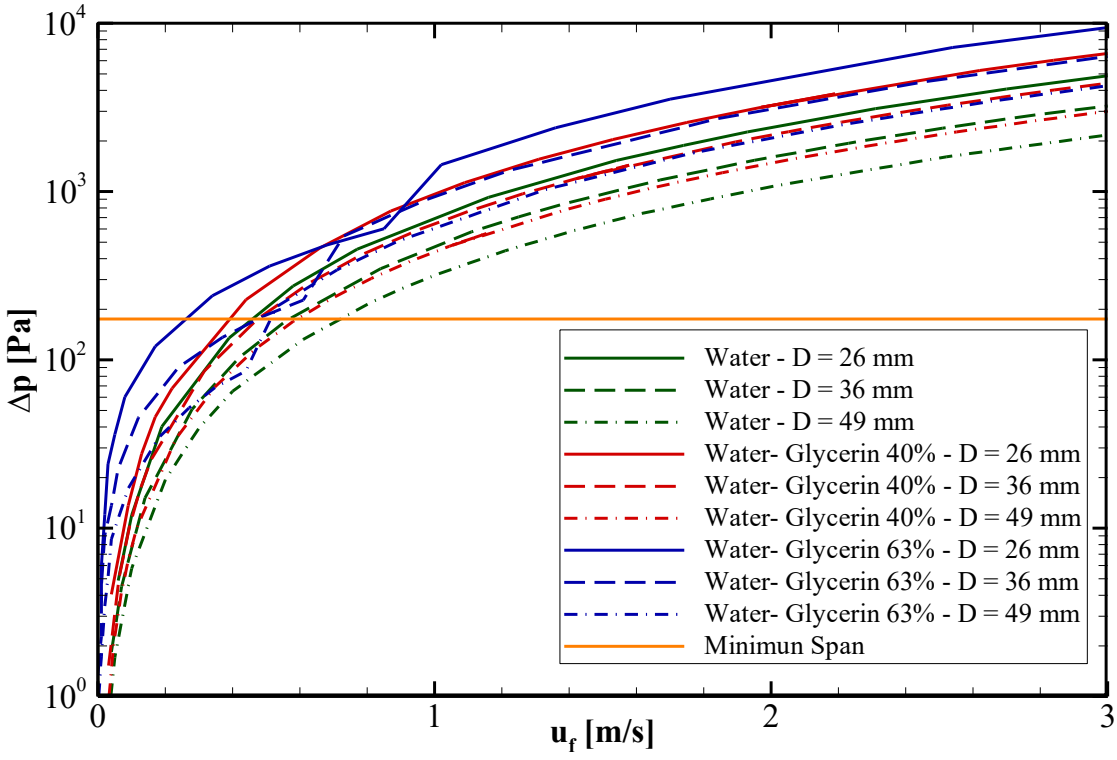

(Source: author)

It is possible to see that for the three fluids, D = 49 mm (represented by the dotted lines) provides a pressure drop significantly below the minimum span, requiring high velocities to reach the minimum value. Therefore, it is more adequate to work either with D = 26 mm or D = 36 mm. However, tests were conducted using plexiglass pipelines with an internal diameter of D = 26 mm, and it was not possible to achieve a condition in which any bed flow pattern was formed.

The pipeline's length aimed to provide the flow development based on the length development criteria, shown in Equation (21) (White, 2010).

$$L_e \approx 1.6\,\mathrm{Re}^{1/4}\,D \tag{21}$$

For the present work, the flow's development length was determined for Re = 150,000, providing a significant security margin compared to the Re values employed. The value was estimated at around 1.15 m. A PVC pipeline with L = 2.5 m is positioned at the entrance of the test section, ensuring flow development and the restriction fulfillment.

Finally, it was estimated that the pump must provide around Δp_{pump} = 3.5 bar at Q = 8 m³/h to achieve the maximum velocity with all fluids. It was employed, then, a Netzsch Helicoidal Pump NM038-BY, which fulfilled the project requirements. The estimative for the pump specification is detailed in Appendix A.

3.3. Step 3 – Experimental Methodology

The methodology employed in the present work is detailed in the present section. The simplifications adopted, as well as the experimental conditions, are justified below.

3.3.1. Experimental Conditions

It was determined that experimental tests should be conducted in fully developed and steady-state conditions, so no transient effects were considered, and the flow pattern detection could be carried out when the liquid-solid flow was statistically stable. Tests with water were conducted to determine the minimum time necessary to collect the data, ensuring the steady-state conditions.

The pump was initially at rest for those tests and then turned on, providing the intended Reynolds number. The time considered for stabilization from the flow start was two minutes and then, data for pressure drop in the test section and the helical pump were stored over twenty minutes. This procedure was repeated for three different values of Reynolds Number (Re = 15,000; 30,000; 45,000). The average of the pressure drop was determined for different time intervals (Δt). The result is shown for both the test section and the pump in Figure 11a and Figure 11b, respectively, where each point represents the average of all Δp values collected over Δt seconds.

Figure 11 – Average pressure drop as a function of the time interval for the (a) test section and (b) the pump.

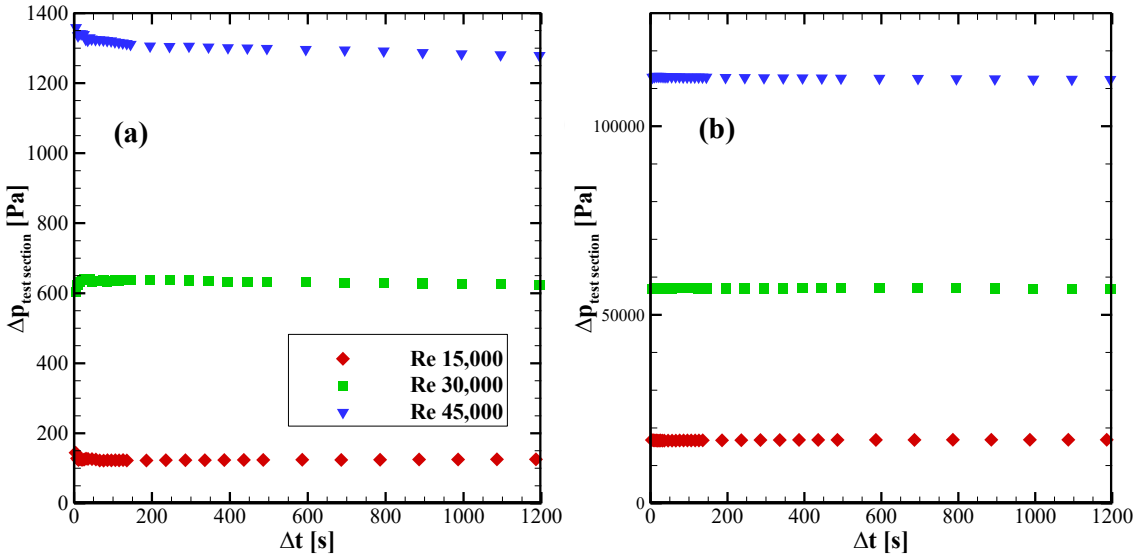

(Source: author).

It can be observed in Figure 11 that the time interval required by the pressure measurement at the pump is significantly smaller than that of the test section. In Figure 11a it is observed that the average of the pressure drop, measured in the test section, was kept constant after Δt = 120s. In Figure 11b, on the other hand, it is noticed that the pressure measured in the pump is constant for all values of Δt. Based on the observations of Figure 11, it was established that 120 s after the pump start, the pressure data was going to be recorded over 300 s, aiming a steady-state and fully developed condition of the flow.

Water and two different water-glycerin concentrations were employed as the working fluids to provide a variation of the dynamic viscosity between tests. The water and water-glycerin mixtures' choices for the viscosity variation are justified by the fluid transparency, which is essential for the flow pattern visual detection. Also, the water and water-glycerin densities are similar, allowing one to isolate the effects of viscosity over the experiments.

Although the water and water-glycerin are considered Newtonian fluids, the dynamic viscosity is sensible to temperature, especially for the water-glycerin mixtures. Since the experimental apparatus does not have a temperature control system, the water-glycerin mixtures' viscosity was characterized as a function of the temperature using a Haake Mars III rheometer with concentric cylinders (CC25 ME Ti). The tests were conducted in triplicate and evaluated the viscosity at T = 15, 20, 25, 30, 35ºC. The result is shown in Figure 12, where each point represents the average of the three tests. The water curve was determined through Equation's correlation (22) (White, 2010).

Figure 12 - Viscosity as a function of the temperature.

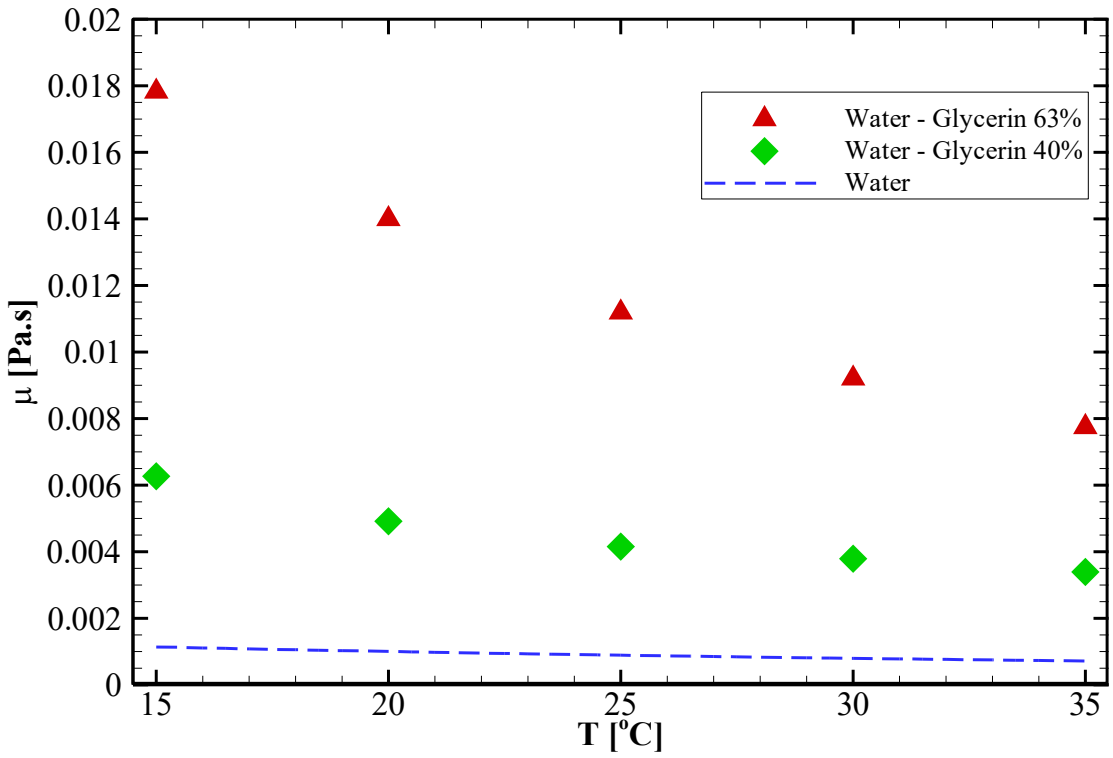

(Source: author).

It was established as a project requirement that the selected fluids provided a variation in the viscosity value of at least one order of magnitude. Figure 12 shows that the variation was greater than one order of magnitude between the water and water-glycerin 63%. The water-glycerin 40% was selected to provide an intermediate reference.

The curve shown for water was not an experimental fit. The viscosity as a function of the temperature was determined through the Equation (22), since the rheometer was unable to work with lower viscosities. T is the temperature in ºC.

$$\mu = 2.414 \times 10^{-5} e^{\left[247.8/((T+273.15)-140)\right]} \quad \textbf{(22)}$$

Data collected for the water-glycerin mixture was fitted using the minimum square method. The correlations and the Equation (22) were inserted in the LabView routine to determine the Reynolds number and the analytical pressure drop properly.

Urea particles with an average size of d_p = 1.44 ± 0.24 mm and density ρ_p = 1480 kg/m³ were employed for the dispersed phase. The particle choice was based on Doron and Barnea (1996) works and Kelessidis and Bandelis (2005). The first work employs polymeric spheres with d_p = 1.5 mm and ρ_p = 1240 kg/m³. However, similar particles' costs were higher than the project budget destined to acquire the solid. Glass spheres similar to those employed by Kelessidis and Bandelis (2005) had ρ_p = 2500 kg/m³, which could exceed the water transport capacity in the system designed. Also, the glass spheres damage the helicoidal pump components due to friction.

The delivered concentration must be kept constant over the experiments to properly evaluate the effects of the viscosity in the flow pattern formation. Therefore, the delivered concentration was fixed at C_s = 3±0,3%wt, which was the highest concentration that was achieved at the lower Reynolds numbers without stopping the helicoidal pump.

The Coriolis flowmeter determined the delivered concentration. Although it does not measure this parameter, it is common to determine it based on fluid density. Over the initial tests, a slightly density variation with the fluid temperature was noticed, affecting the concentration determination. Therefore, the effects of the temperature on the density were evaluated for each fluid. The evaluation used the system designed, where the pump was started, and the density data were collected by the *Coriolis* flow meter until the

temperature was significantly increased. The procedure was repeated for all three fluids, and the result is shown in Figure 13.

Figure 13 - Density as a function of the temperature for the (a) water; (b) water glycerin 40% and (c) water-glycerin 63%.

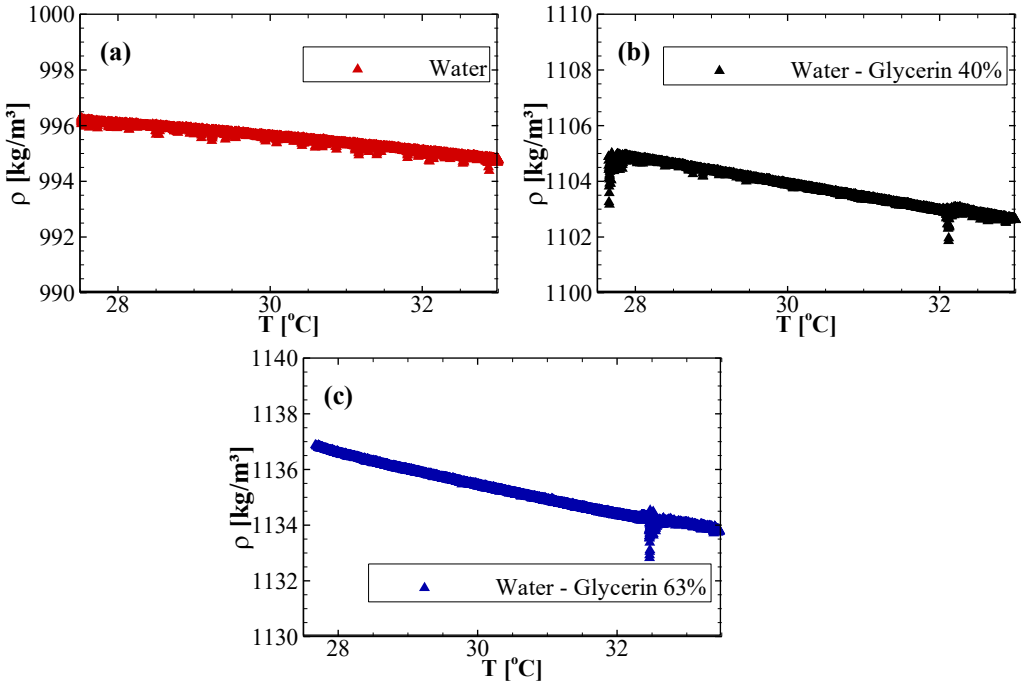

(Source: author).

The points collected were fitted with the minimum squares method, and the fit was implemented in the LabView routine to determine the delivered concentration properly.

3.3.2. Test procedure

The working fluid was prepared at the mixing tank, and the flow means velocity was set to the lowest Reynolds number established for the given fluid. Then, bubbles were removed from the system and the pressure transducer pipeline. Once the velocity was stable, the liquid-solid mixture was prepared at the mixing tank. To fulfill the requirement of delivered concentration $C_s = 3\pm0{,}3\%$wt, the particles were injected in the system until the desired condition was achieved. 120 s after the pipeline was filled with the biphasic flow, and the delivered particle concentration was fixed, the data was collected for 300 s.

Completed the test, the Reynolds number was increased to the next step of the test matrix. However, if the Re was increased, the delivered concentration changed with the

fluid velocity, just as expected (Doron and Barnea, 1995). Thus, the next Reynolds number established was set, and the particles were manually removed from the system until the C_s = 3±0,3%wt requirement was achieved. The procedure was repeated for every experimental condition conducted in triplicate, aiming to evaluate data deviation.

3.3.3. Data treatment

With the collected data, a flow pattern map was developed in which the pressure drop per unitary length was plotted as a function of the Reynolds number The detection of all three flow patterns was expected, allowing it's representation on the flow pattern map. The suspension flow is assumed to be a heterogeneous flow at all cases, since the equipment available for the study is unable to detect the transition between the heterogeneous suspension and the pseudohomogeneous suspension.

The transition between two flow patterns happens anywhere between two experimental points, as illustrated in Figure 14a. Therefore, a transition point is defined at the average position between the two experimental points closest to the transition, as illustrated in Figure 14a. The methodology was be repeated for all fluids studied and a curve fit was developed between all points representing the transition between two specific flow patterns. The resulting curve should represent each flow pattern boundary, as represented in Figure 14b.

Figure 14 – Graphical representation of a) the transition point defined according to the criteria described and b) a fitted curve for multiples transition points.

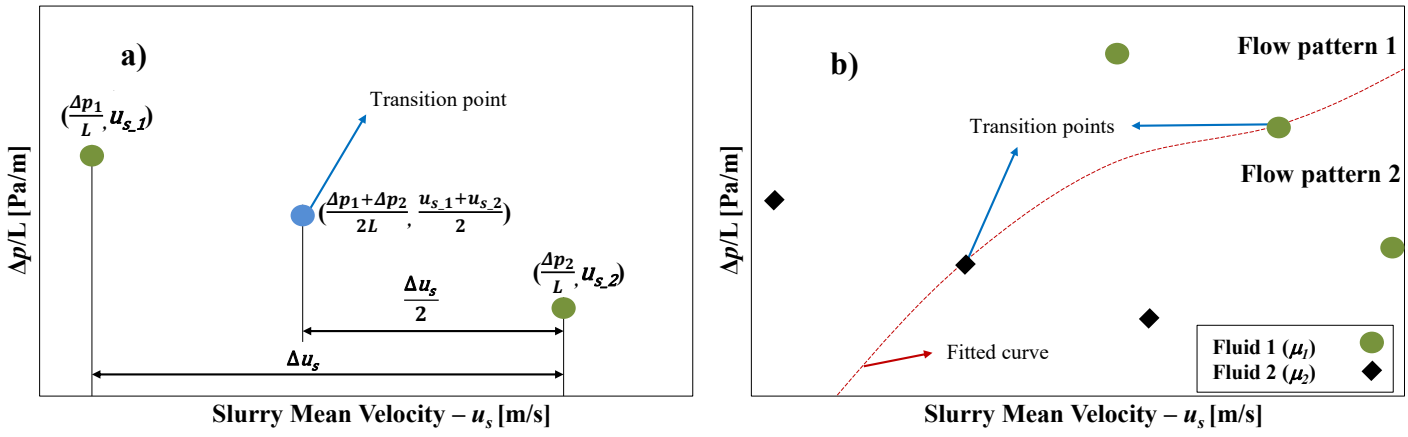

(Source: author).

The development of the flow pattern map should allow one to predict the flow pattern in which a pipeline is submitted by measuring the slurry mean velocity and pressure drop per unitary length, as long as the fluid viscosity and solids concentration are known.

3.3.4. Uncertainties Analysis

The collected data uncertainty evaluation was based on the ISO GUM (2008) standard for uncertainties.

Through measuring devices and sensors, any data experimentally obtained necessarily implies uncertainties related to each instrument's precision. Therefore, uncertainty analysis is essential to identify potential error sources or quantify the results' precision and validity (Fox and McDonald, 2011).

Experimental uncertainties may be divided into two principal causes: systematic and random errors. Systematic errors are related to an average deviation, compared to an expected value, and are minimized through equipment calibration. Random errors, however, are associated with data dispersion and cannot be corrected. Therefore, random uncertainties are estimated using statistical tools (White, 2010).

ISO GUM (2008) standard defines the error estimation by dividing them between type A and type B uncertainties, which are individually detailed below.

3.3.4.1. Type A Uncertainties Analysis

Type A uncertainties (δ_A) are associated with data dispersion and are expressed through the standard deviation value (s), determined through Equation (23), where n is the sample number, x_j represents each value measured and $\bar{x}$ is the mean (ISO GUM, 2008).

$$\delta_A\left(x_j\right) = s\left(\bar{x}\right) = \sqrt{\frac{1}{n-1}\sum_{j=1}^{n}\left(x_j - \bar{x}\right)^2} \quad \textbf{(23)}$$

3.3.4.2. Type B Uncertainties Analysis

Type B uncertainties (δ_B) are related to equipment precision, a constructive characteristic of each measuring device. Therefore, the ISO GUM (2008) standard suggests that this information is obtained with the manufacturer or from each device's calibration certificates.

3.3.4.3. Combined Uncertainties

For a single variable, the combined uncertainty is determined based on the values of type A and type B uncertainties and is estimated by Equation (24) (ISO GUM, 2008).

$$\delta = \sqrt{\delta_A{}^2 + \delta_B{}^2} \tag{24}$$

It is also possible to determine the uncertainty of an arbitrary parameter T, which is dependent on *n* measured variables. Equation (25) presents an expression employed to estimate the arbitrary parameter T's random uncertainties, depending on each variable's combined uncertainty δx_n (White, 2010).

$$\delta T = \left[\left(\frac{\partial T}{\partial x_1} \delta x_1 \right)^2 + \left(\frac{\partial T}{\partial x_2} \delta x_2 \right)^2 + \ldots + \left(\frac{\partial T}{\partial x_n} \delta x_n \right)^2 \right]^{1/2} \tag{25}$$

The determination of the uncertainties in the present work is discussed in Appendix B, in which each parameter and its type B uncertainties are mentioned.

3.3.5. Test Matrix

The test matrix is shown in Table 7 and was developed based on the Reynolds number on the test section. It was intended to evaluate different Reynolds number ranges with each fluid. The minimum limit was established as the lowest Reynolds, in which it was possible to achieve C_S = 3%wt without blocking the pump. The maximum limit was the highest volumetric flow rate, where intense vibrations were avoided in the system. The test matrix shows the conditions tested for each fluid and the parameters raised for each test.

The test matrix presents how the tests will be conducted regarding the Reynolds number the equivalent average mixture velocity. Although each fluid contemplates different Re ranges, the velocity range is similar for the three fluids.

Table 7 – Test matrix

Fluid	Re	u_m [m/s]
Water-Glycerin 63%wt	1,000	0.31
	2,000	0.61
	3,000	0.92
	4,000	1.22
	5,000	1.53
	6,000	1.84
Water-Glycerin 40%wt	4,000	0.38
	5,000	0.48
	7,500	0.72
	10,000	0.96
	12,500	1.19
	15,000	1.44
Water	20,000	0.56
	30,000	0.84
	40,000	1.11
	50,000	1.39
	60,000	1.67
	70,000	1.95

(Source: author)

Each experimental condition presented in the test matrix was conducted in triplicate, so the data deviation was evaluated, resulting in 54 experiments developed for the study conclusion.

3.4. Step 4 – Experimental apparatus assembly

The experimental apparatus was assembled in the facilities of the Research Center for Rheology and non-Newtonian Fluids (CERNN)[7], according to the project proposed in Subsection 3.2.

[7] The research center is located at the Federal University of Technology in Paraná (UTFPR).

The assembled experimental rig is shown in Figure 15a, and the test section is detailed in Figure 15b. The flow direction follows the red signals and the position of the test section is indicated in Figure 15 by the orange square. The test section is at the end of the pipeline in order to ensure the flow development length.

Figure 15 – a) Experimental rig and b) detailed test section.

a) **b)**

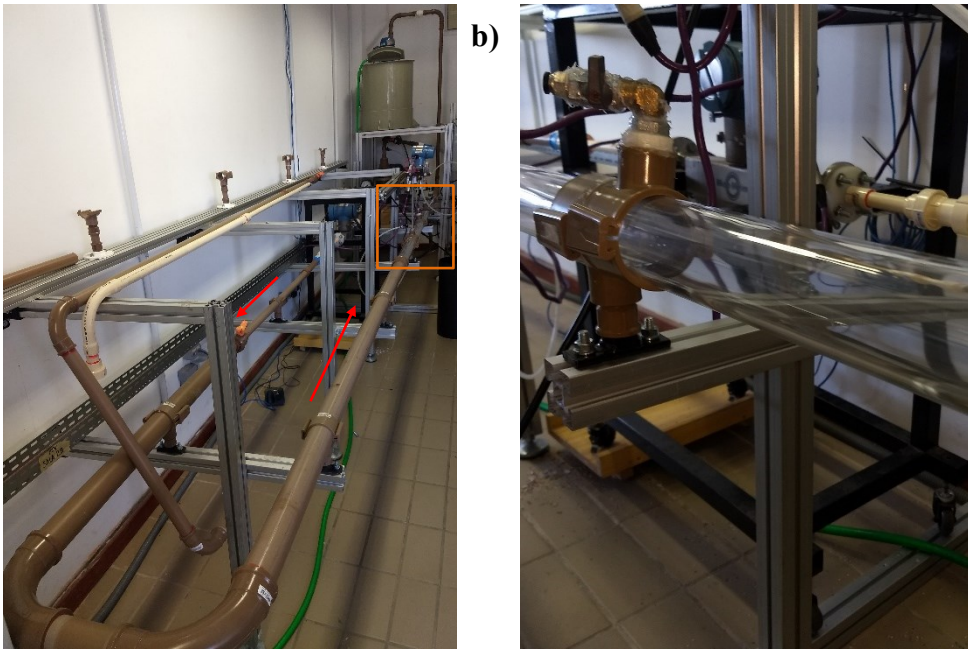

(Source: author).

The helicoidal pump was positioned at the bottom of the tank. Over the assembly process, it was necessary to ensure that the pipeline inclination, or height difference, did not happen before the test section's differential pressure measurement. The increase in the pipeline height happened only after the test section in returning to the mixing tank.

3.5. Chapter Synthesis

In the present chapter, the most relevant steps of the methodology were described. A dimensional analysis was developed, where the Euler number should describe the present work as a function of the Reynolds number. The experimental setup was designed, and the most important instruments were detailed in the section. The experimental procedure employed for the flow pattern map development was described, where the transition is characterized by pressure drop and Reynolds number measurements.

Three fluids with different viscosities were employed for the viscosity effect's evaluation: water, water-glycerin 40%wt and water-glycerin 63%. The density and viscosity of each fluid were characterized as a function of the temperature. Finally, the test matrix was presented described the conditions of each one of the 54 tests developed.

4. RESULTS AND DISCUSSION

Collected data and results are displayed and discussed in the present chapter. The chapter was divided into four sections:

a) Apparatus validation.
b) Description and discussion of the collected images.
c) Pressure drop results and flow pattern maps.
d) Power consumption.

Each section and the containing results will be discussed below.

4.1. Apparatus validation

The pressure transducer was calibrated with a *Fluke 718 300G* pressure calibrator to ensure that the differential pressure measurement in the test section was trustworthy,. The calibration curve is shown in Figure 16, where the error bars represent the combined uncertainties.

Figure 16 – Pressure measured by the pressure transducer versus the pressure provided by the pressure calibrator.

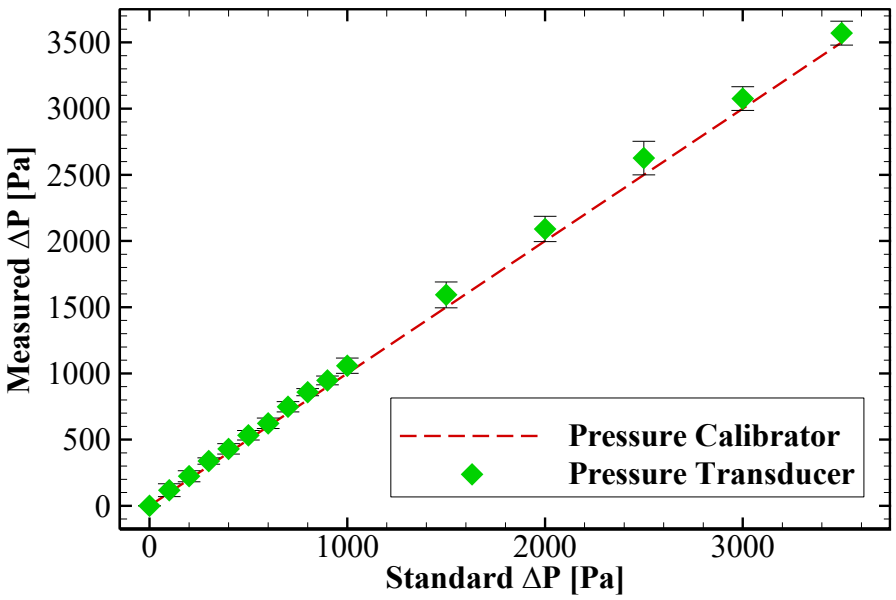

(Source: author).

In Figure 16, the dashed red line represents the pressure calibrator's standard pressure, while the green symbols are the values measured by the pressure transducer. As it can be observed, the pressure drop collected by the pressure transducer is close to that provided by the pressure calibrator, where the highest relative error was in the order of 11% for pressure drop values lower than 200Pa.

Even after the calibration, it was necessary to ensure that the differential pressure measurement was trustworthy in measuring the experimental bench flow pressure loss. Therefore, the pressure drop was measured in the proposed test section for a monophasic flow condition and then compared with the pressure drop analytical determination for cylindrical pipelines. The analytical estimative for the pressure drop was based on Equation (5). The fluid properties and other parameter's values were measured experimentally for the analitycal estimative.

The fluids employed were the three fluids proposed in section 3.3. The Reynolds number range was based on the test matrix's values, shown in Table 7. In order to estimate the friction factor, the Blasius correlation was employed. The result is shown in Figure 17.

Figure 17 – Pressure drop measured in the test section Experimental apparatus analytical validation for monophasic flow.

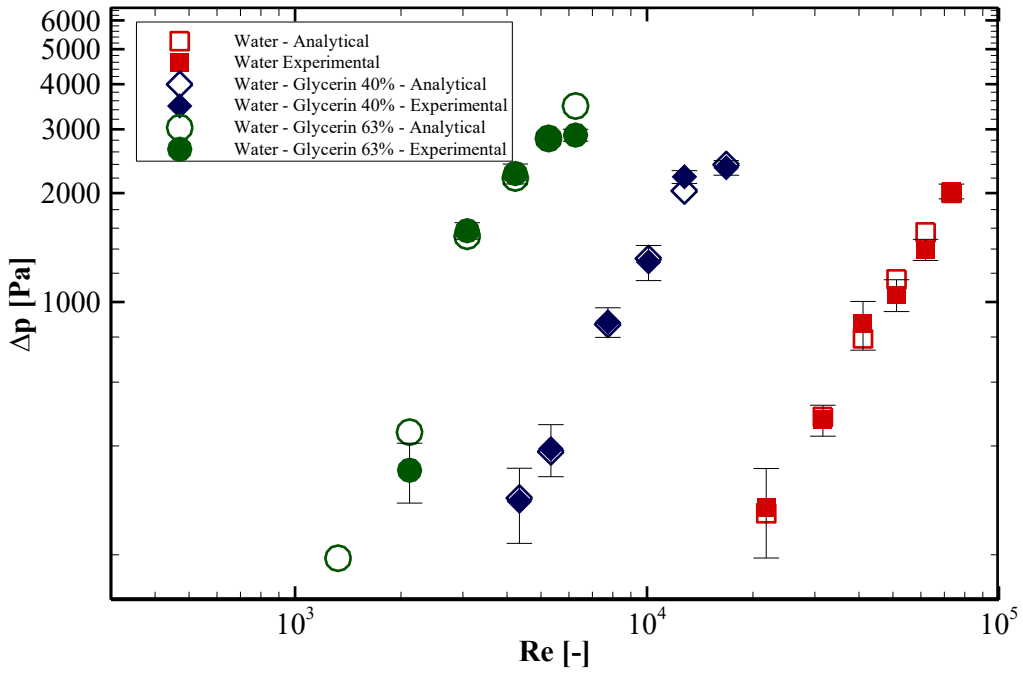

(Source: author).

The hollow symbols represent the pressure drop analytical estimation for the fluid flow, while the filled symbols represent the test section's pressure measurement. It can be noticed that for all cases, the difference between the measured pressure drop and the analytical estimative does not exceed 15%.

It must be mentioned that the curve shape for the water-glycerin mixtures presents unexpected path changes when compared to the water, due to high sensitivity of the glycerin dynamic viscosity with temperature variations. Along with the tests, the fluid temperature increases significantly due to viscous dissipation, which decreases the fluid dynamic viscosity. Since the experimental bench control is based on the Reynolds number in the test section, the fluid velocity must be increased to keep the non-dimensional parameter fixed. This velocity variation results in pressure drop changes. However, the objective was to validate the equipment, which is not affected by this phenomenon.

4.2. Description and discussion of the collected images.

The present section aims to discuss each experimental condition's flow pattern based on the flow visualization's qualitative information. The determination of the flow pattern transition is necessary in order to establish the flow pattern map.

For the discussion, one image is shown for each experimental condition employed. The images are shown for all experimental conditions tested and all working fluids.[8]

The images collected over the experiments are presented in Table 8, Table 9 and Table 10, where each experimental condition is indicated.

Table 8 presents the images corresponding to the tests conducted with water. It can be noticed that only the flow pattern observed at Re = 20,000 presented three layers. Figure 18 indicates each layer and presents the estimated interface between them. As detailed in Figure 18**,** the bed formed at the bottom of the pipeline contains two different layers, the bottom layer was considered a stationary bed, and the upper layer is considered a moving bed. Although the bottom layer was considered as a stationary bed, the layer is slipping on the pipeline wall. This layer's distinctive characteristic, which indicated it as

[8] For more accurate evaluation of the images, the videos collected can be watched in the link https://alunosutfpredubr-my.sharepoint.com/:f:/g/personal/tiagov_alunos_utfpr_edu_br/EtqKrGql3ElGmj_hWkB9zJoBHOjet8KN3LzKIPyzLYuAFw?e=XfsTLe

a stationary bed, is that the particles moved as a plug. Apparently, there is no relative velocity between the particles, indicating that the movement occurred similarly to a solid element displacement. However, the upper layer is clearly a moving bed layer, where the fluid continuously drags the particles on the top of the bottom layer. The upper layer movement is not uniform, where dunes are often formed for particle transport, which is expected, according to Doron and Barnea (1987) and Kelessidis and Bandelis (2005) descriptions of the moving bed formation. Finally, a heterogeneous suspension is present above the moving bed.

Table 8 - Images captured during the experiments using water as the working fluid.

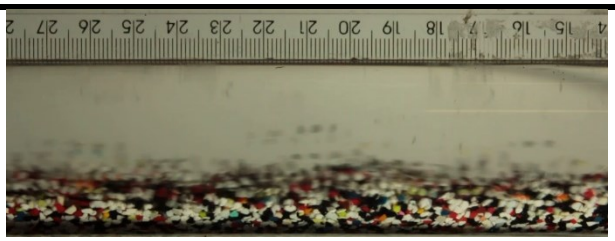	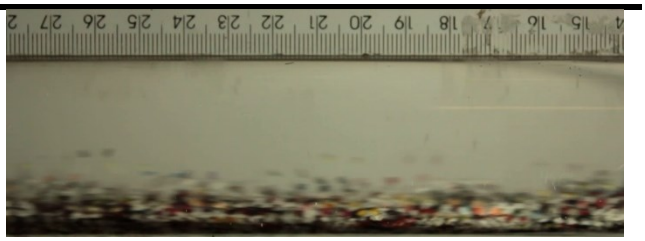
Re 20,000	Re 30,000
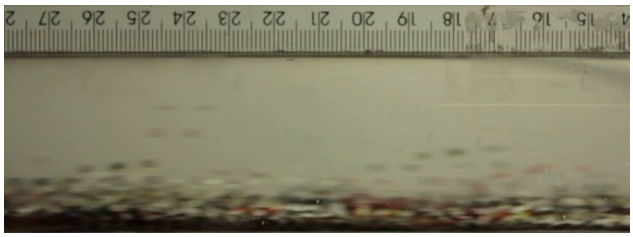	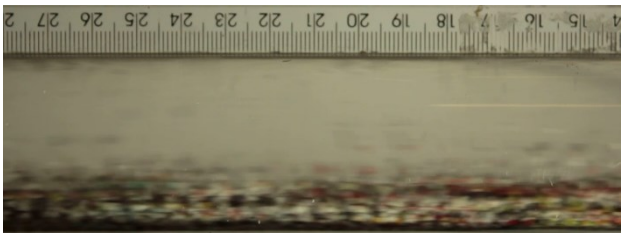
Re 40,000	Re 50,000
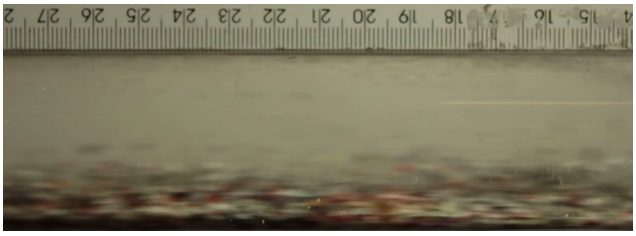	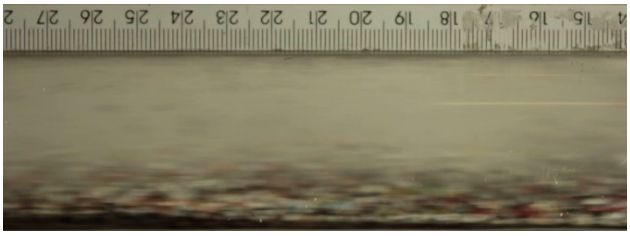
Re 60,000	Re 70,000

(Source: author)

Figure 18 – Detail of the flow with a stationary bed, indicating the (a) stationary bed layer, (b) moving bed layer and (c) heterogeneous flow for Re = 20,000 employing water as the working fluid.

(Source: author).

While Re = 20,000 was the only water condition that indicated a stationary bed formation, it was observed for Re = 30,000 that the flow pattern had already transitioned to a two-layer flow.

Over the experiments, it was noticed that the camera's frame rate was not able to capture the particle movement for all experimental conditions properly. Starting at Re 40,000, it was not possible to determine if the particles were touching the pipeline wall, which should establish if the flow pattern already transitioned to a heterogeneous suspension flow or still behaved as a moving bed flow. It was observed a low number of suspended particles at Re = 70,000, compared to the highest Reynolds number employed for the other fluids (Re = 15,000; Re = 6,000), which happens on a similar velocity range. This behavior leads to the assumption that the flow was not yet suspended. The images of those conditions can be observed in Table 9 and Table 10, respectively. However, the image analysis does not provide a conclusive result, lacking the pressure drop evaluation for more discussion, developed at Section 4.3.

Table 9 presents one image for each experimental condition for the water-glycerin 40%wt tests. It was observed a flow with a stationary bed at both Re = 4,000 and Re = 5,000, where the height of the stationary bed was decreased as Re was increased, shown in more detail in (Source: **author)**

Figure 19. The decrease in the bed height was already expected due to the transition from flow with a stationary bed to flow with a moving bed. For the transition, the stationary layer's particles will be dragged as the mean velocity is increased, reducing the stationary bed until only a moving layer is detected at the bed. Also, the stationary layer's slipping velocity is almost negligible at Re = 4,000, compared to Re = 5,000. This is probably due to the stationary layer's highest height at Re = 4,000, which required a higher pressure drop to move the stationary bed layer.

At Re = 7,500, a moving bed flow was already observed, which indicated that the flow pattern transitioned at some point between Re = 5,000 and Re =7,500. Once more, the camera framerate prevented the image analysis of the highest Reynolds numbers. From Re = 10,000, it is not possible to observe the particles and assess whether they are in contact with the bottom surface of the pipeline or not.

Table 9 – Images captured during the experiments using water-glycerin 40%wt as the working fluid.

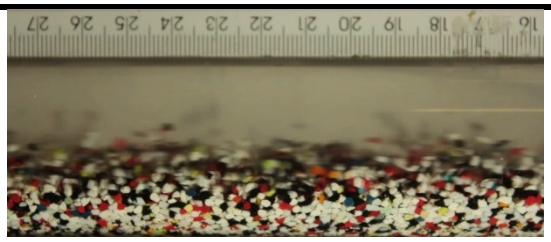	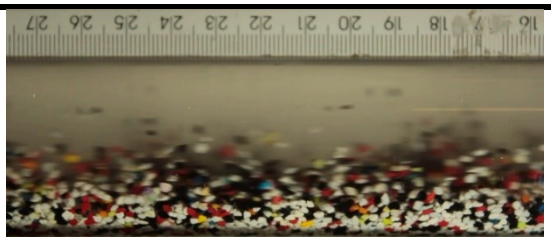
Re 4,000	Re 5,000
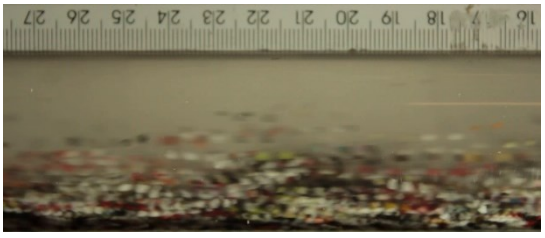	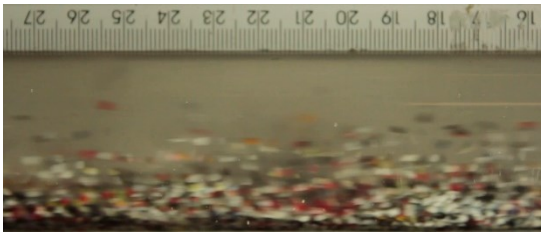
Re 7,500	Re 10,000
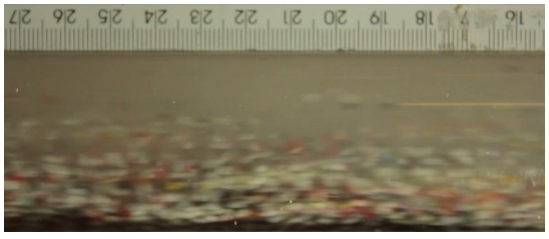	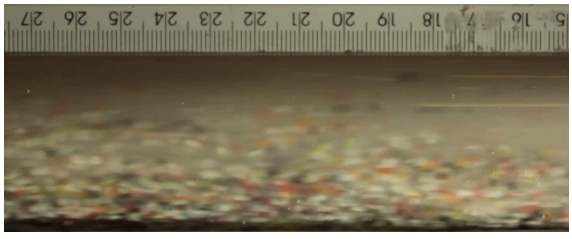
Re 12,500	Re 15,000

(Source: author)

Figure 19 – Detail of the flow with a stationary bed, indicating the stationary bed layer, moving bed layer and heterogeneous flow for a) Re = 4,000 and b) Re = 5,000 employing water-glycerin 40%wt mixture as the working fluid.

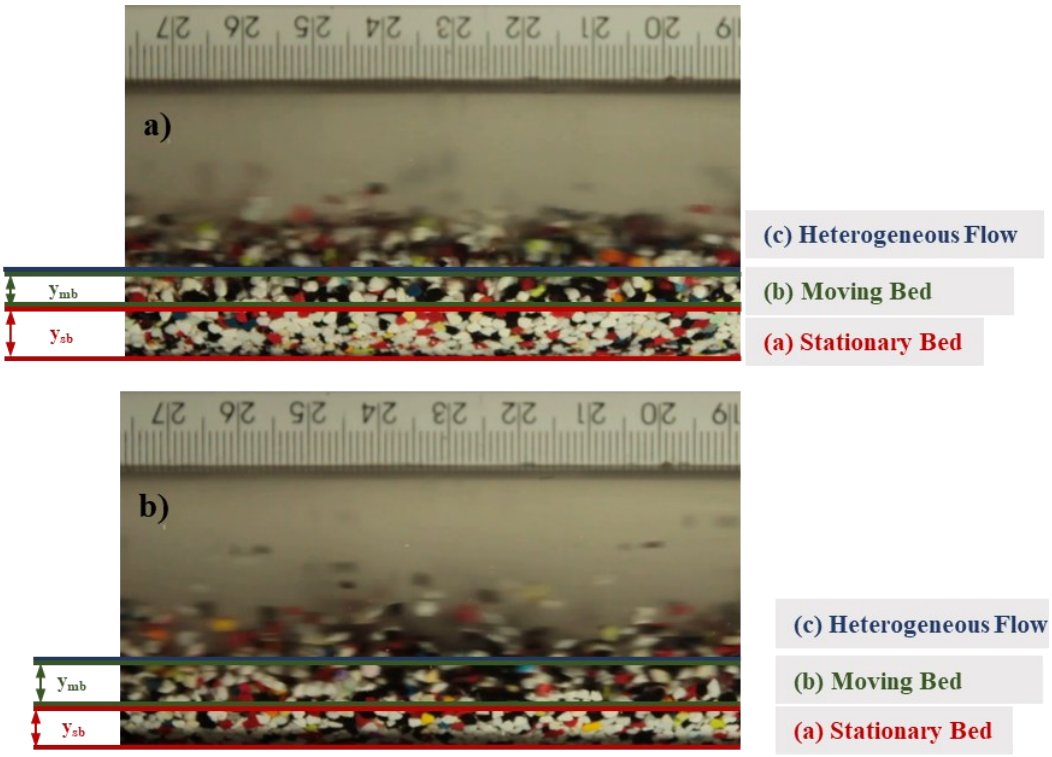

(Source: author).

Images collected for the water-glycerin 63%wt are presented in Table 10. A flow with a stationary bed was observed only at Re = 1,000, detailed in

Figure 20. The flow with a moving bed is already present at Re = 2,000, indicating that the transition happened somewhere between both conditions. Starting at Re = 3,000, it was impossible to evaluate the images due to the framerate limitation accurately.

For all fluids tested, it was possible to determine the region in which the transition from the flow with a stationary bed to flow with a moving bed happened. Slipping effects on the bed's stationary layer were noticed for most cases in which a flow with a stationary bed was present.

It was observed that particle rotation is responsible for the solid's movement on the boundary between the stationary and moving bed layers. The phenomenon agrees with Kelessidis and Bandelis (2005) description of the erosion process in the bed. The authors proposed that the erosion is induced by the fluid action over the particles at the stationary bed's surface, on the boundary between the bed's stationary and moving layers. Based on Doron and Barnea's (1993) model, developed through shear stress balances on the interface between the layers, it is conjectured that a minimum shear stress value is necessary to provide the particle movement.

Table 10 – Images captured during the experiments using water-glycerin 63%wt as the working fluid.

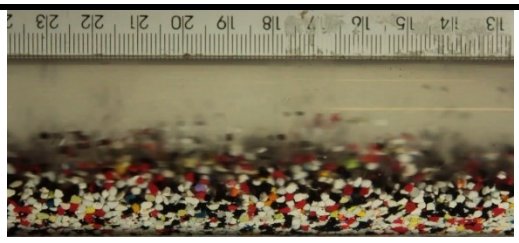	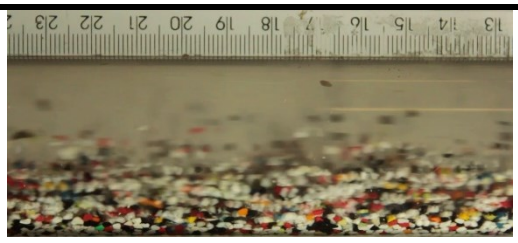
Re 1,000	Re 2,000
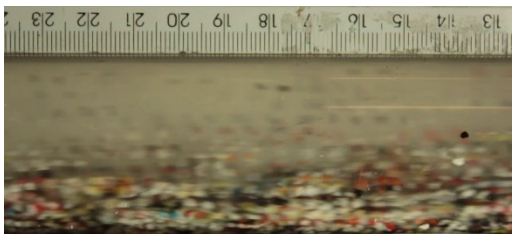	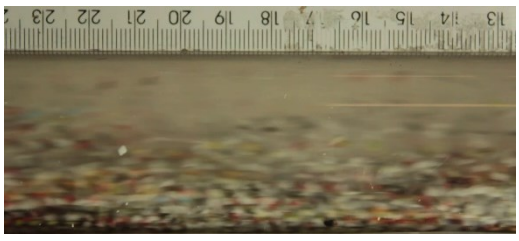
Re 3,000	Re 4,000

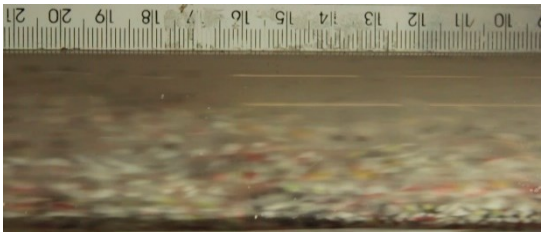

Re 5,000

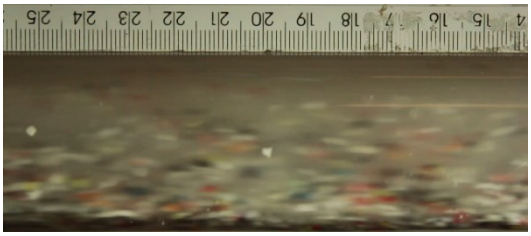

Re 6,000

(Source: author)

Figure 20 – Detail of the flow with a stationary bed, indicating the (a) stationary bed layer, (b) moving bed layer and (c) heterogeneous flow for Re = 1,000 employing water-glycerin 63%wt as the working fluid.

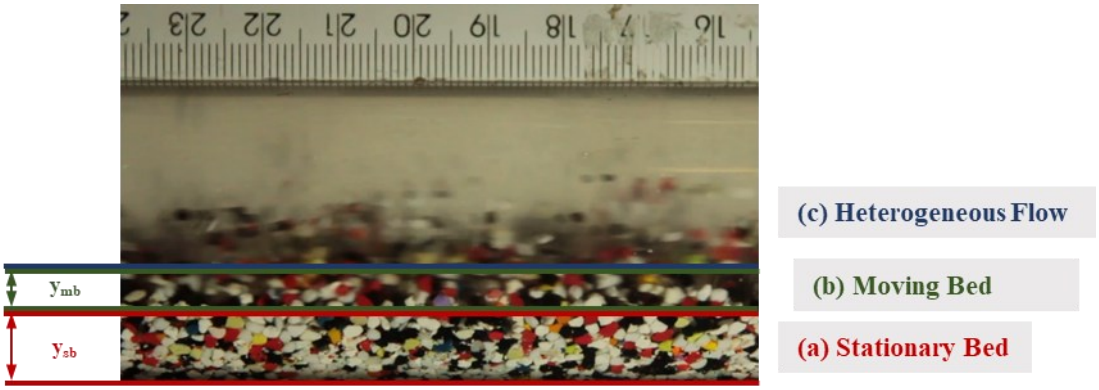

(Source: author).

The transition from flow with a stationary bed to flow with a moving bed was detected through visualization. The camera framerate was unable to properly detect the particles at higher mixture velocities and the transition to heterogeneous suspension was undefined for all fluids. The Reynolds number and mixture velocities equivalent to the region of transition are shown in Table 11. The Reynolds number for the stationary bed represents the last experimental coordinate from the test matrix in which the mentioned

flow pattern was observed for that given fluid. The value indicating the moving bed characterizes the first experimental condition in which the flow pattern was detected.

Table 11 – Transition from the flow with a stationary bed to flow with a moving bed.

Fluid	Stationary Bed	Moving Bed	Heterogeneous Suspension
Water	Re = 20,000 u_m = 0.46 m/s	Re = 30,000 u_m = 0.65 m/s	Undefined
Water-Glycerin 40%	Re = 5,000 u_m = 0.48 m/s	Re = 7,500 u_m = 0.68 m/s	Undefined
Water-Glycerin 63%	Re = 1,000 u_m = 0.34 m/s	Re = 2,000 u_m = 0.53 m/s	Undefined

(Source: author)

Due to the designed methodology, the transition between the stationary bed flow to a moving bed flow is not established by a single point for each fluid but is represented by a region between two experimental points.

Table 11 shows that the required Reynolds number for the transition from stationary bed to moving bed is significantly different for each fluid, which is expected due to the test matrix design. However, the velocity requirement is much closer. In particular, the differences between the water and water-glycerin 40% velocities are almost negligible. Although the velocity required for the transition is decreased for the water-glycerin 63%, when compared to the other fluids, there is an intersection between the transition region on the three fluids from u_m = 0.48 m/s to u_m = 0.53 m/s. This suggests that the transition from the flow with a stationary bed to flow with a moving bed dependence relies more on the flow velocity than on the fluid viscosity.

4.3. Pressure drop

The pressure drop is a commonly used parameter for industrial flows in general. Therefore, the evaluation of the effects of the viscosity variation on the pressure drop was

developed. The pressure drop was also chosen as one of the flow pattern map representation parameters due to its use on industrial systems.

The pressure drop measured in the test section is presented in the dimensional form in Figure 21 as a Reynolds number function. In the graphic, the measured pressure drop per unitary length is compared with the monophasic analytical estimation. The experimental biphasic data average is represented by the filled symbols and the analytical estimative by hollow symbols.

Figure 21 – Comparison between pressure drop for biphasic flow and monophasic analytical estimative.

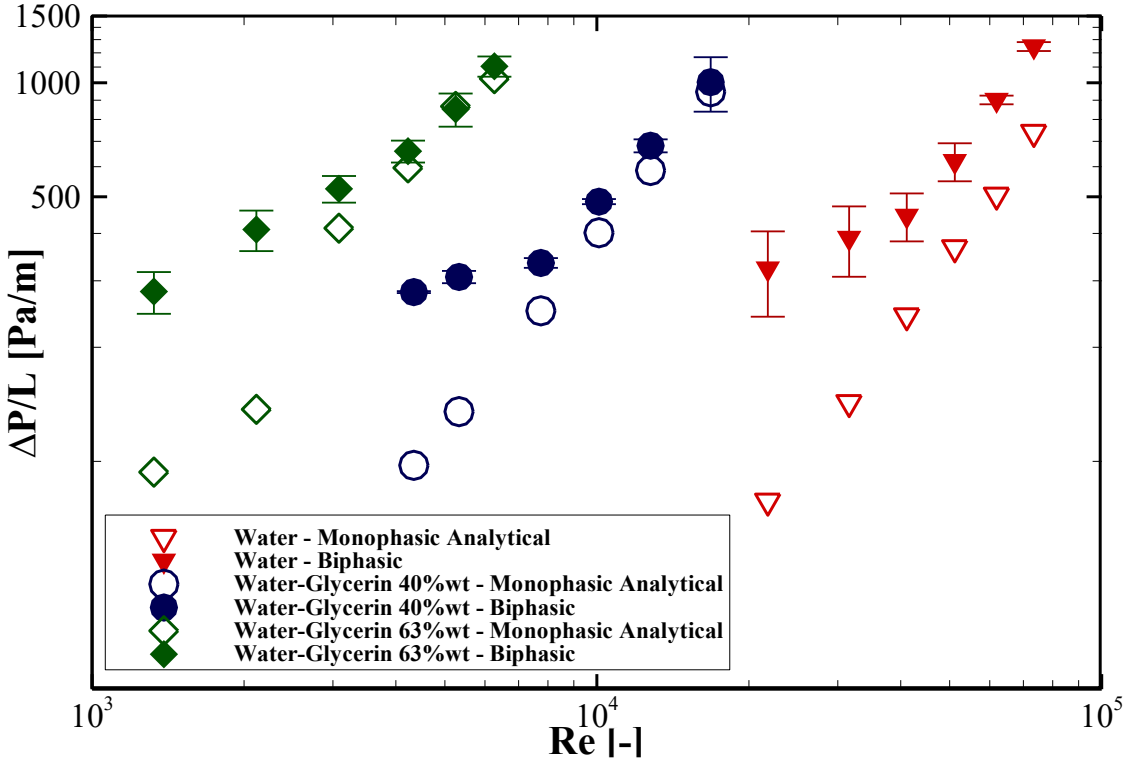

(Source: author).

The analytical calculation was developed in the *Labview* environment, where the measured parameters fed the analytical expression for the pressure drop, shown in Equation (5), allowing the monophasic pressure drop determination for fluid properties similar to those experimentally tested.

It is noticeable in Figure 21 that the monophasic behavior of the water-glycerin 63%wt is significantly different from the other fluids. That is justified due to the transition from laminar to turbulent flow between Re = 2,000 and Re = 3,000. The friction factor determination changes significantly with the regime transition, modifying the pressure loss curve.

Based on the comparison between the monophasic and biphasic pressure drop, insights on the flow pattern transition should be taken. In general, it is expected that the pressure drop is higher than that of the monophasic flow since the bed acts as an area reduction element for the flow with a stationary bed. With the flow pattern transition to flow with a moving bed, the pressure drop difference between the biphasic and monophasic flows is decreased. As the moving bed transitions to a heterogeneous suspension, the biphasic pressure drop tends to the monophasic value since there is no

bed to act as a pressure loss source (Kelessidis and Bandelis, 2005). Although the experimental conditions were distinct, the behavior observed in Figure 21 is similar to the observed by Kelessidis and Bandelis (2005), described above.

It is observed in Figure 21 that the pressure drop per unitary length magnitude is similar for the three fluids. Except for the water-glycerin 63%wt, it is noticed that there is a significant change in the slope of the data dispersion tendency, reducing the pressure drop difference between the monophasic and biphasic values.

A sudden slope change is observed for the water-glycerin 40%wt, which coincides with the flow pattern transition from the flow with a stationary bed to the flow with a moving bed, in agreement with the image evaluation. The variation on the tendency inclination is smoother for the water and happened near the region where the moving bed was achieved, although it does not coincide precisely with it. The water-glycerin 63%wt variation in the slope was probably not observed due to the flow regime transition from laminar to turbulent flow.

The slope change was expected close to the flow with a moving bed development (Kelessidis and Bandelis, 2005). The agreement with the literature description provided more credibility to the image interpretation for the stationary and moving bed.

For the transition from the flow with a moving bed to the heterogeneous suspension, it is necessary to analyze the tendency of the biphasic pressure drop measurement approximation to the monophasic value after the flow with a moving bed was achieved. Starting with the water, it is noticed that, even for Re = 70,000 the pressure drop is significantly distinct from the monophasic value, indicating that the fluid was unable to suspend the particles for the condition tested, corroborating the assumption adopted on image analysis. For both water-glycerin mixtures, it was noticed that the monophasic and biphasic curves overlapped, suggesting that the flow pattern transitioned to a heterogeneous suspension.

To estimate precisely when the heterogeneous suspension was achieved, a linear fit was developed through the minimum squares method for the biphasic flow pressure drop data. The process neglected data representing the stationary bed condition. The analytical estimative for the pressure drop, the experimental data, and the linear fit are shown in Figure 22.

Figure 22 – Estimative of the transition between the flow with a moving bed and the heterogeneous suspension.

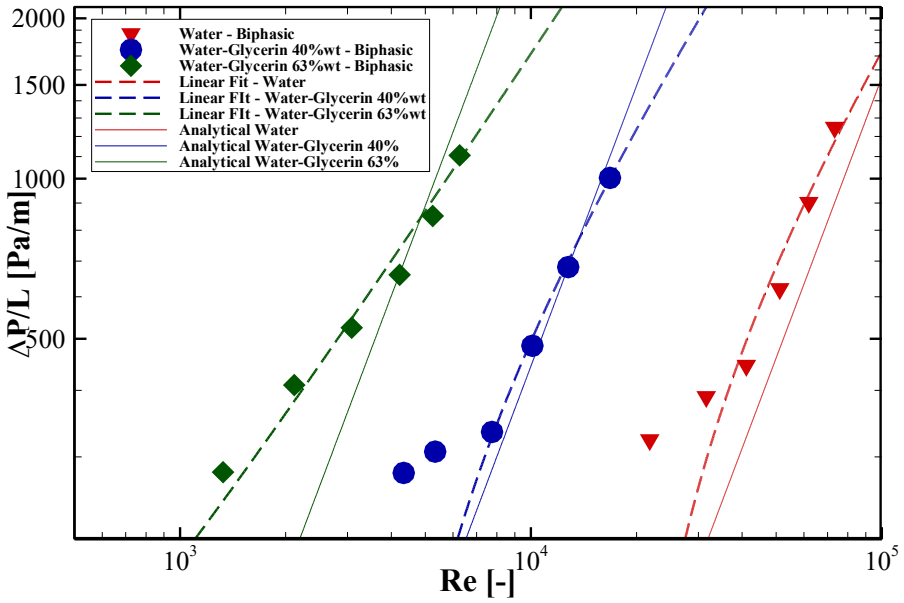

(Source: author).

As it can be noticed from Figure 22, there is a point in which the monophasic and biphasic pressure drops have the same value. Kelessidis and Bandelis (2005) indicate that the biphasic pressure drop tends to the monophasic as the suspension flow is reached. Therefore, the present study assumed that the required Reynolds number for the heterogeneous suspension happened at the intersection between the linear fit and the monophasic analytical estimative.

The correlations for the pressure drop and the analytical expressions for monophasic turbulent flow were matched for the value determination, and the resulting equation was solved for the Reynolds number. The resulting value of Re represented the requirement for heterogeneous suspension of the particles.

The linear adjustment has the form of

$$\Delta p = B.(\mathrm{Re}) + C \qquad \textbf{(26)}$$

The constants B and C's values, determined through data fit, are shown in Table 12 for each fluid. The Re necessary for the flow pattern transition into a heterogeneous suspension is presented in the same table with its equivalent u_m.

Table 12 – Estimative of the Reynolds number necessary for the heterogeneous suspension transition and the equivalent average mixture velocity.

Fluid	Re	u_m [m/s]	*B* [Pa]	*C* [Pa]
Water	121,984	3.06	0.021	-367.31
Water-Glycerin 40%	13,412	1.29	0.074	-253.97
Water-Glycerin 63%	4,860	1.19	0.169	23.405

(Source: author)

It can be noticed that fluid viscosity changed the transition from the moving bed to the heterogeneous suspension, where higher viscosity required smaller mixture velocities to achieve the flow configuration. The required velocity was reduced in 15% from the water-glycerin 40%wt to the water-glycerin 63%wt. The suspension was not achieved for the water in the present work; however, the water curves' point should cross was estimated. However, it cannot be ensured that the correlation accurately represents the problem beyond the data fitted since it has no physical meaning.

The dimensionless pressure drop, represented by the Euler number (Equation 11), is expressed as a function of Re in Figure 23. It can be noticed that the Eu behavior is similar for all fluids employed in the present work. The high values of Eu at low Reynolds number evidenced that inertial effects are less prevalent than the pressure loss due to the flow restriction. Since bed flows (stationary and moving) happened at low Re, the assumption that the bed acts as a significant pressure loss source is corroborated. Also, increases in the Reynolds number reduced Eu, as more particles are suspended, and the dynamic pressure effect becomes more prevalent. This behavior is seen as the dimensionless pressure drop tends to the unity with the solids suspension.

Figure 23 – Dimensionless pressure drop as a function of the Reynolds number.

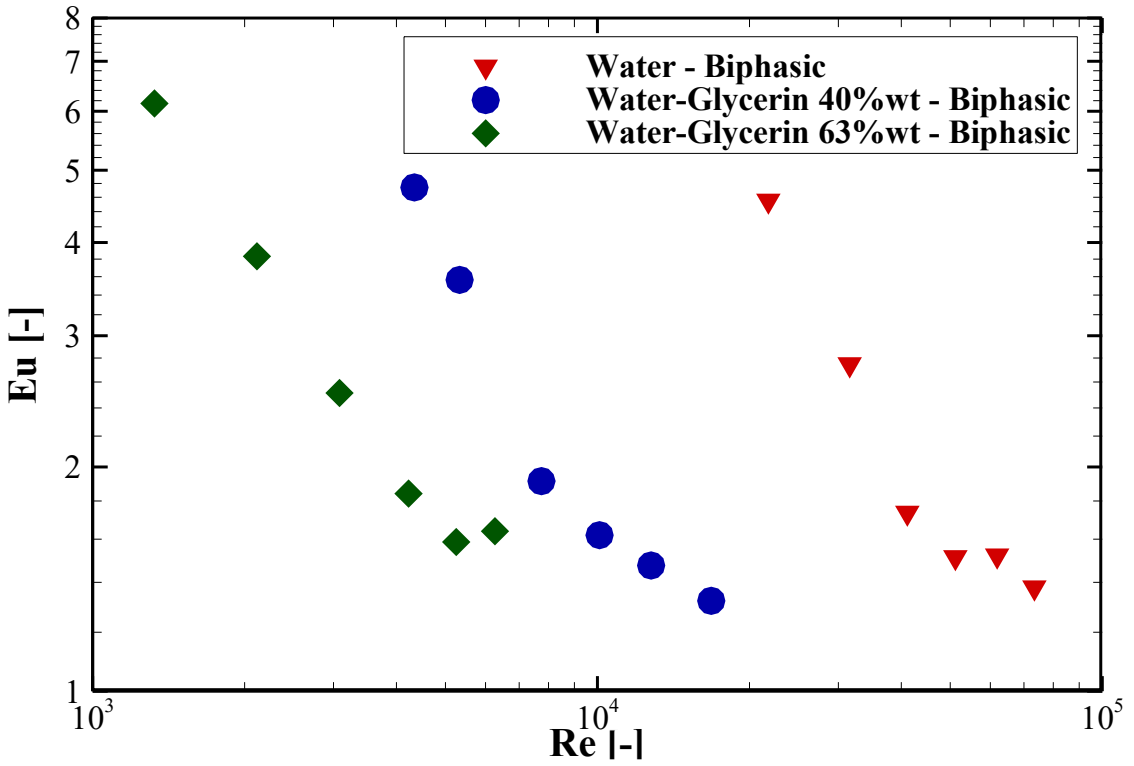

(Source: author).

Both the dimensional and non-dimensional pressure drops were represented as a function of the average mixture velocity in Figure 24a and Figure 24b, respectively. Defining u_m as the independent parameter provides a set of coordinates with a similar range on the *x*-axis for the three fluids, which does not occur when the independent variable is the Reynolds number. This condition allows a more precise evaluation of the fluid change effects on the biphasic pressure drop. It can be observed that the pressure drop per unitary length increase due to the viscosity variation is significant for the biphasic flow. Differences of up to 22% were observed between the water and water-glycerin collected data. However, the Euler number variation was almost negligible, where the points seemed to display a single curve.

Figure 24 – a) Dimensional pressure drop per unitary length as a function of u_m and b) non-dimensional pressure drop as a function of u_m.

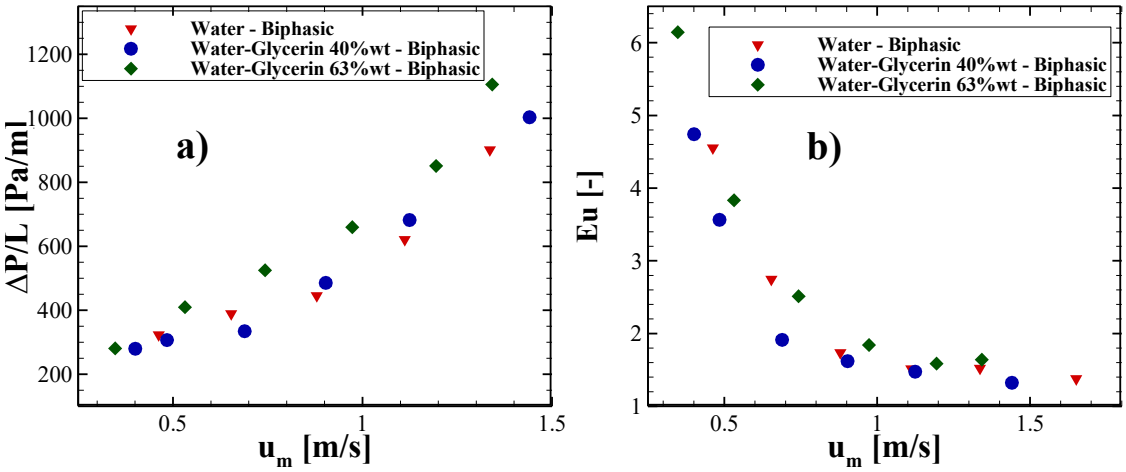

(Source: author).

The dimensional analysis development showed that Froude's number should influence the studied problem. Therefore, the Euler number is shown, in Figure 24, as a function of Fr.

Figure 25 – a) Dimensional pressure drop per unitary length as a function of u_m and b) non-dimensional pressure drop as a function of u_m.

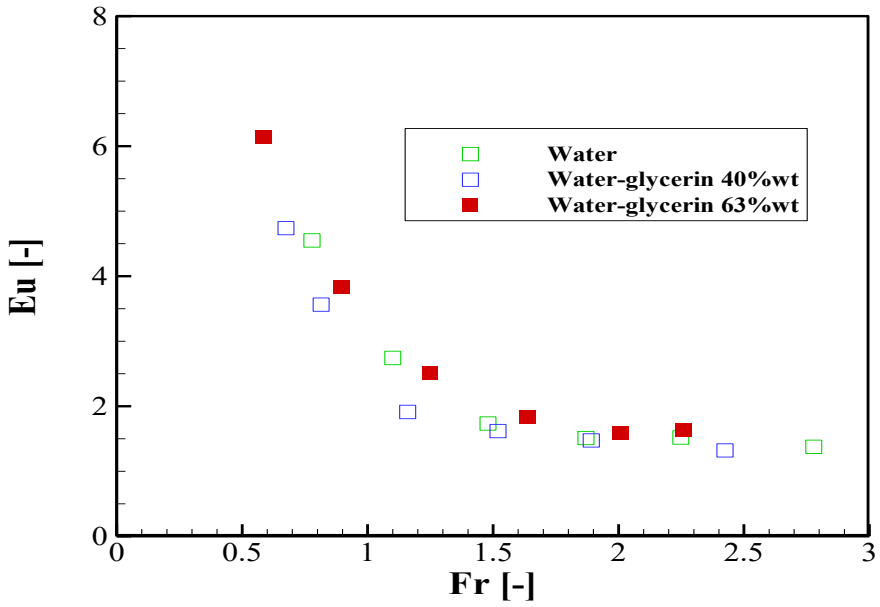

(Source: author).

As it can be noticed, Eu and Fr are inversely correlated. The Eu number decreases as Fr is increased. Fr represents the correlation between flow inertia and field effects, represented by the present problem's gravitational field. The behavior described suggests that field effects are more prevalent at higher values of Eu, where the particles acting as an area reduction element are more relevant. Therefore, it is supposed that flow inertia effects over particles are significant. However, the effects of fluid viscosity are not accounted for by either of the dimensionless groups discussed above. Therefore, the difference between the Eu (Fr) curves can be considered negligible. Also, it is important to notice that the curve behavior is similar to Eu(u_m) behavior since the only parameter that changes over the tests is u_m.

Finally, the required Re for all flow pattern transitions and its equivalent u_m, are summarized in

Table 13 for each fluid studied in the present work. The values presented in the table were employed to develop the graphical representation of the flow pattern map, shown in Figure 26.

Table 13 – Transition between flow patterns based on the value of the Reynolds number and u_m.

	Stationary Bed – Moving Bed	**Moving Bed – Heterogeneous Flow**
Water	Re = 26,701 u_m = 0,56 m/s	Re = 121,984 u_m = 3.06 m/s
Water Glycerin 40%wt	Re =6,539 u_m = 0,58 m/s	Re = 13,412 u_m = 1.29 m/s
Water-Glycerin 63%wt	Re = 1,720 u_m = 0,44 m/s	Re = 4,860 u_m = 1.19 m/s

(Source: author)

Once the region in which the transition between the flow patterns probably occurred was determined, the flow pattern map could, finally, be developed and graphically represented in Figure 26. The points represent the experimental data, while the dashed lines denote the transition between the flow patterns indicated in the figure.

The dashed lines that represent the flow regime change were determined through a linear fit employing the minimum squares method. Since the transition stationary to moving bed flow was detected through visualization, the data fit was developed using the average point between the first and last condition that each flow pattern was observed, as proposed in Section 3.3.3 and illustrated in Figure 14. However, for the moving bed to heterogeneous suspension, the points were defined based on the u_m values presented in

Table 13. To properly develop the data fit, an ordinate pair (Δp, u_m) is necessary. Therefore, an exponential data fit was developed for each fluid, and the equivalent pressure drop was estimated for the transition.

Figure 26 – Flow pattern map indicating the regime transitions as a function of the flow pressured drop, Reynolds number, and dynamic viscosity.

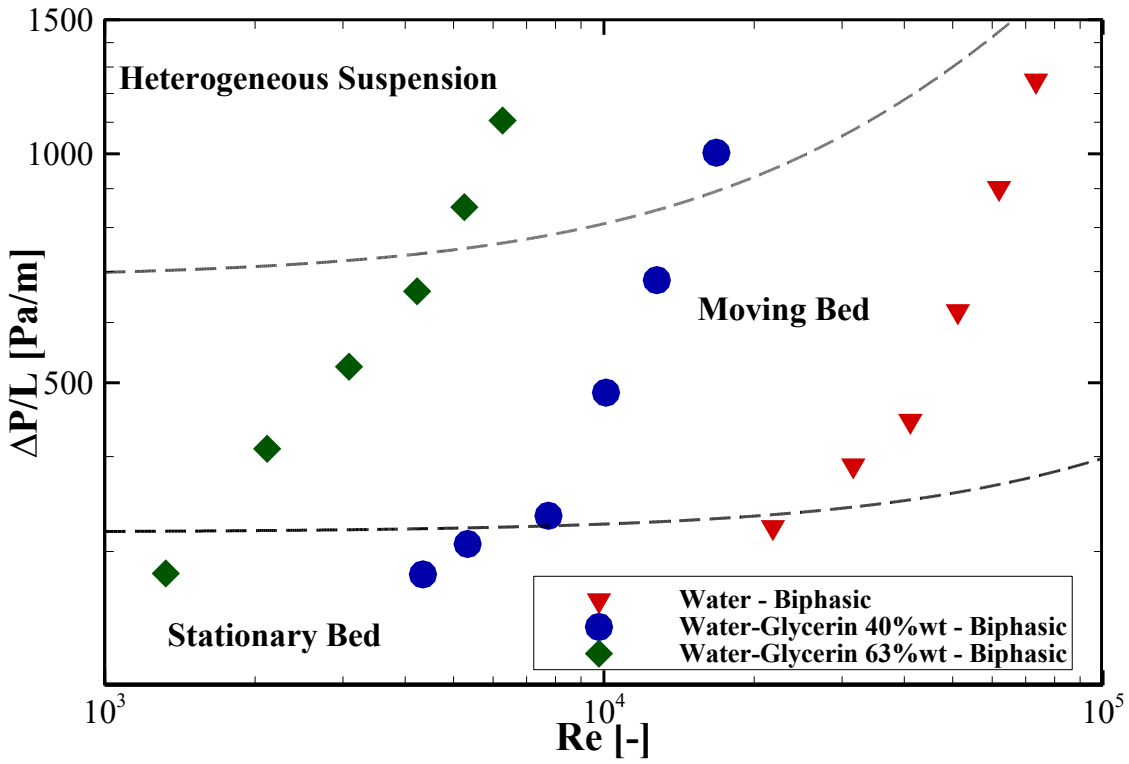

(Source: author).

It can be observed in Figure 26 a similar behavior for the curves representing the three different fluids. The pressure drop curve was displaced to the left as the fluid viscosity was increased. In the flow pattern map presented, the transition for a specific fluid is characterized by the intersection between the linear fits, expressed by dashed lines, and the pressure drop tendency for that fluid. Once the data displayed represents constant viscosity curves, it is possible to assume that lower viscosity fluids required a higher Reynolds number for both transitions, and the opposite is analogous.

It was noticed that the variation on the fluid properties affected both flow pattern transitions. Although the influence of the viscosity variation on the stationary to moving bed transition was more discret, the transition from the flow with a moving bed to the heterogeneous suspension was greatly affected by the fluid property. Evaluating the results from

Table 13 together with Figure 26, it is observed that the requirement for flow pattern transition was increased, as the viscosity was decreased. The water required higher values of Δp and u_m to provide the particle suspension. The opposite behavior is equivalent, where the increase in the viscosity is provided with lower Δp and u_m to achieve the heterogeneous suspension. It is also noticed that for both transitions, the viscosity effect becomes more prevalent at higher values o Re, where the curve inclination is more pronounced.

The variation on the Reynolds requirement for the heterogeneous suspension development was only at the order of 15% between the water-glycerin mixtures. However, it was not possible to reach the heterogeneous suspension when water was employed. This behavior is probably explained by the flat-shaped particles employed in the study. According to Miedema and Ramsdell (2016), flat-shaped particles tend to deposit with the smaller cross-section area perpendicular to the flow direction. Kelessidis and Bandeli's (2005) description of bed erosion establishes that the impact erosion is more prevalent for low viscosity fluids, such as the water, where the particle suspension is mostly caused by the fluid impact over the exposed area of the solid elements. Once the exposed area presents a small cross-section area, the impact cannot lift and carry the particles, explaining why the water could not reach the suspension. However, as the

viscosity is increased, the shear erosion becomes more relevant in such a condition that the exposed area of the particle is not as important.

Miedema and Ramsdell (2016) proposed that higher fluid velocity is required to provide flat solids suspension. However, the present study indicates that lower fluid velocities may reach the same flow configuration as long as the fluid viscosity is significantly increased. Due to the particles' irregular shape, the authors suggested that particle rotation over the bed should be noticed before the suspension, which was indeed the case.

Peker and Helvaci (2011) suggested that the momentum diffusion caused by the fluid turbulence provides a support mechanism, which opposes the particle suspension's gravity action. However, it was observed that Re = 70,000 did not suspend more particles than lower values of Re for the water-glycerin mixtures. Significantly lower values of Re achieved the heterogeneous suspension, which was not possible for the water.

The hypothesis that turbulence is the most important phenomena for particle suspension at horizontal pipelines seems incomplete. The water flow reached Re = 70,000 and, yet, the suspension was not developed. Fluid properties also have a significant influence on particle suspension. It is well established that fluid density is a relevant variable due to its direct proportionality in the buoyancy force determination (Doron et al., 1987; Nazari et al., 2010). However, the present work shows that the dynamic viscosity also seems essential for solids transportation in horizontal pipelines.

Understanding the need for a correlation for pressure drop estimating liquid-solid flows that explicitly represent the dynamic viscosity effects, the present work proposed a correlation based on the collected data. Therefore, an exponential fit was developed for the data shown in Figure 26. Then, each fluid was represented by an exponential fit with the form of Equation (27).

$$\frac{\Delta p}{L} = Ke^{M\,\mathrm{Re}} \qquad \textbf{(27)}$$

The constants K and M were determined through the minimum squares method for each fluid, meaning that different fluids should be represented by different equations. However, the correlation development aimed the pressure drop estimative as a function

of the fluid viscosity for different fluids. Therefore, a linear interpolation was developed, between the constants *K* and *M* and fluid properties. The resulting value for the constants should provide a equation that properly fits the data for fluids with different properties. Since the density slightly changes between the fluids employed in the present work, the development was based on the kinematic viscosity ν, which accounted for both the fluid density and viscosity, $\nu = \frac{\rho}{\mu}$.

Since three fluids were employed, the interpolation was based on the fluids' properties with the highest and lowest values of ν. The intermediate fluid was then employed to validate the correlation results.

The interpolation allowed one to determine the constants based on the Equations (28) and (29).

$$K = K_{water} + \left(\nu - \nu_{water}\right)\left[\frac{K_{water} - K_{water-glycerin63\%}}{\nu_{water} - \nu_{water-glycerin63\%}}\right] \quad \textbf{(28)}$$

$$M = M_{water} + \left(\nu - \nu_{water}\right)\left[\frac{M_{water} - M_{water-glycerin63\%}}{\nu_{water} - \nu_{water-glycerin63\%}}\right] \quad \textbf{(29)}$$

The generic constants *K* and *M* are determined as a function of a generic fluid properties, represented by ν, the properties of the fluids studied in the present work and the constants obtained with the minimum squares method for each fluid. The terms inside the square brackets are constant and were replaced by generic constants *K'* and *M*' in the deduction.

$$K = K_{water} + \left(\nu - \nu_{water}\right)K' \quad \textbf{(30)}$$

$$M = M_{water} + \left(\nu - \nu_{water}\right)M' \quad \textbf{(31)}$$

However, the values of *K'* and M_{water} are not user-friendly, being too high or too low. Therefore, it was decided to represent the equation as a function of the generic fluid properties and the water properties, a standard reference. Therefore, *K'* was represented by the ratio $K' = \frac{K''}{\nu_{water}}$ and M_{water} was represented by the product $M_{water} = M''.\nu_{water}$, where

K'' and *M''* are constants. The generic constants are, then, given by Equations (32) and (33).

$$K = K_{water} + (\nu - \nu_{water}) \frac{K''}{\nu_{water}} \quad \textbf{(32)}$$

$$M = M''.\nu_{water} + (\nu - \nu_{water}) M' \quad \textbf{(33)}$$

Finally, after some algebra, the constants are determined by Equations (34) and (35).

$$K = K_{water} + \left(\frac{\nu}{\nu_{water}} - 1 \right) K'' \quad \textbf{(34)}$$

$$M = M''.\nu_{water} + \nu(M' + M'') = M''.\nu_{water} + \nu M_i \quad \textbf{(35)}$$

Replacing Equations (34) and (35) in Equation (27):

$$\frac{\Delta p}{L} = K_{water} + \left(\frac{\nu}{\nu_{water}} - 1 \right) K'' e^{(M''.\nu_{water} + \nu M_i)\mathrm{Re}} \quad \textbf{(36)}$$

Finally, replacing the constants based on the fluids properties and the exponential fit, the correlation becomes

$$\frac{\Delta p}{L} = 165.43 + \left(\frac{\nu}{\nu_{water}} - 1 \right) 5.42 e^{(2.97.\nu_{water} + 26.97\nu)\mathrm{Re}} \quad \textbf{(37)}$$

The verification of the results obtained from the correlation is presented in Figure 27. Symbols represent the experimental data, while the solid lines express the correlation results.

Figure 27 – Comparison between the results obtained with the proposed correlation and the experimental data: a)as a function of the Reynolds number and b) based on the ΔP/L experimental value.

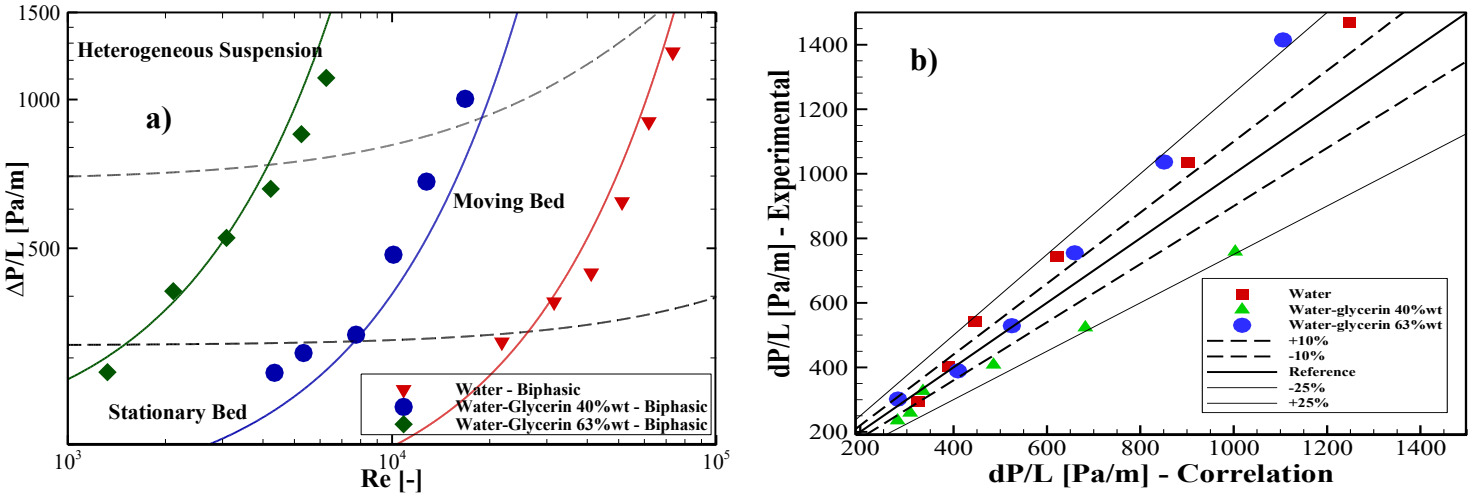

(Source: author).

As it can be noticed, the correlation estimative is close to the experimental measurement. The error is more significant for the water glycerin-40%wt due to the linear interpolation characteristics since the adjustment ensures more precision on the boundary data. On Figure 27b, it can be noticed that data inclination for water and water-glycerin 63%wt are very similar, where the errors are around 20%. As mentioned above, the water-glycerin 40%wt error is more relevant, leading to a line inclination very distinct from that of the other fluids. However, the error modulus is maintained under 25% from reference.

The effects of ν were evaluated using the correlation proposed in Equation (37) to analyze the results' general behavior when employed kinematic viscosities different from the values experimentally studied. The results are presented in Figure 28, where different values of ν were employed. The dashed-dotted lines are the fluids experimentally evaluated and the solid lines represent generic fluids to provide the kinematic viscosity variation. The value of ν stipulated for the intermediate lines was defined as the average value of the real fluid's kinematic viscosity.

The qualitative behavior of the pressure drop is similar to those obtained for the three fluids experimentally validated. The correlation seems well behaved, even for values that surpassed the boundary of the fluids employed. However, further tests are necessary to ensure the precision of the correlation.

Figure 28 – Evaluation of the effects of ν developed through the pressure drop correlation.

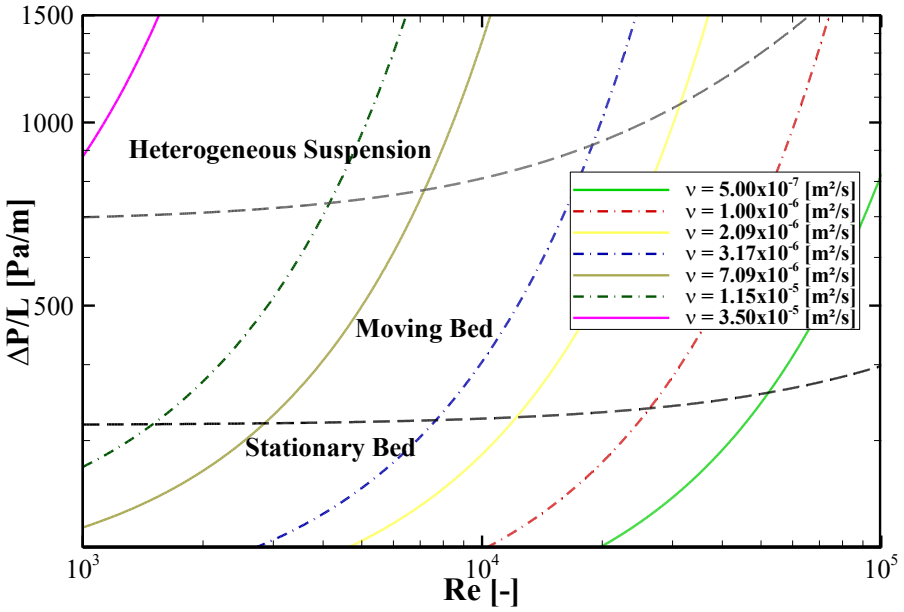

(Source: author).

4.4. Power Consumption

The pressure drop provided by the helical pump was measured, aiming the determination of the power consumption. The system pressure drop is shown as a function of both the pressure drop and the Reynolds number in Figure 29.

Figure 29 – Pressure gradient provided by the pump in the system represented as a function of the a) Reynolds number and the b) mixture average velocity.

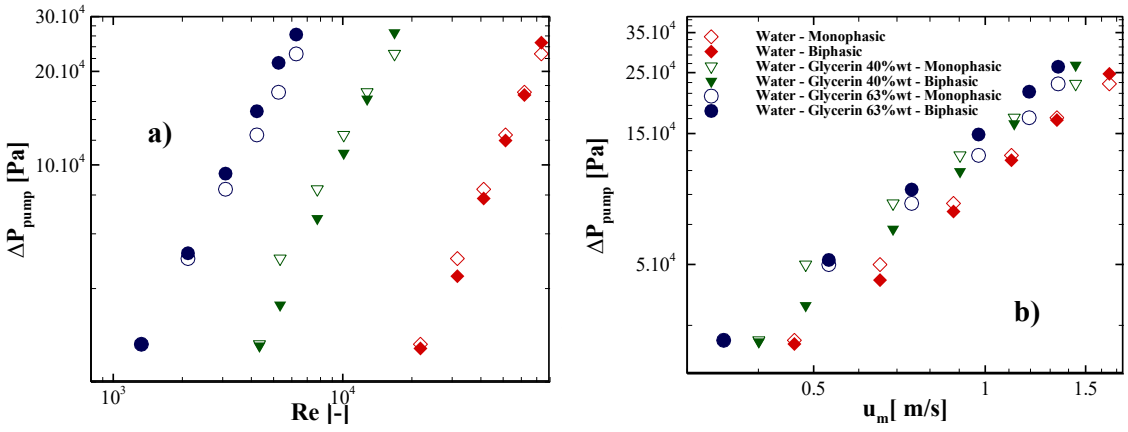

(Source: author).

The difference between the monophasic and biphasic pressure drop is almost negligible, as can be noticed in both graphics. In Figure 29b it is observed that the viscosity difference provides a significant variation on the pressure drop. However, the presence of the particles does not increase the measured pressure drop. The parameter measurement difference can probably not be evaluated due to its greater order of magnitude compared to data collected at the test section.

Power consumption is shown in Figure 30a as a function of the mixture mean velocity. As expected, the power consumption is higher for the fluid with greater dynamic viscosity. The difference in the power required by the system increases with the fluid velocity. At lower velocities, the difference is negligible and increases as the system's flow rate is raised.

The same parameter is shown in Figure 30b as a Reynolds number function, indicating the flow pattern transition region. It can be observed that lower dynamic viscosity allows one to achieve a flow with a moving bed at lower power consumption. However, it is the opposite regarding particle suspension. Although the power consumption was lower while operating with water, the velocity required to achieve a heterogeneous suspension is much greater than that of the other fluids, causing the power consumption to increase significantly compared to the other fluids.

Although the consumed power is lower for low viscosity fluids, these materials may consume higher power to avoid bed formation, resulting in pipeline blockage.

Figure 30 – Power consumption as a function of the a) mean mixture velocity and b) the Reynolds number.

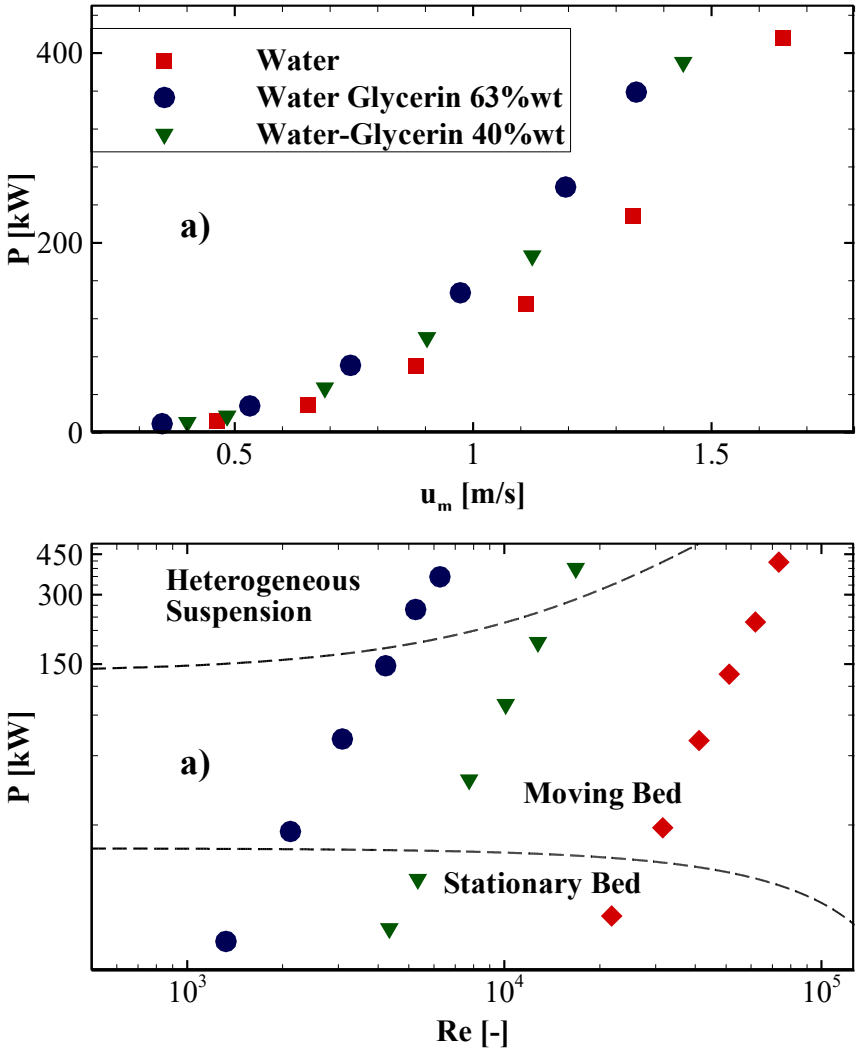

(Source: author).

5. FINAL CONSIDERATIONS

The prediction of flow patterns in industrial applications is a matter of major concern to avoid expensive problems in the system, leading to the pipeline's total blockage. Flow pattern maps can be experimentally developed as one alternative to predict the flow patterns in industrial pipelines. Effects of fluid's viscosity in flow pattern transition was the main goal of this work.

A dimensional analysis was developed at a first moment, resulting in Eu and Re as the most relevant parameters for the problem described. In the sequence, an experimental apparatus was designed and assembled in CERNN facilities. Similarly, an experimental methodology was proposed and employed for data collection. Regarding the fluids employed, water and two water-glycerin mixtures were used to provide the viscosity variation. The parameters Δp and ρ_f were characterized for each fluid as a function of the temperature. Urea particles with an average size of d_p=1.44mm and ρ_p = 1480 kg/m³ were employed as the solid phase.

The apparatus instruments were successfully calibrated and compared with a monophasic pressure drop analytical calculation. The agreement between the experimental data and the analytical estimative was considered satisfactory, where relative errors were smaller than 15%.

The transition between the stationary bed and the moving bed was visually detected based on the collected images. However, the heterogeneous suspension transition could not be visually detected due to the camera framerate limitation. Therefore, a criterion was developed to estimate the transition based on comparing the monophasic and biphasic pressure drop measurements. Based on these statements, a flow pattern map was developed.

Based on the flow pattern map, it was observed that the effects of the fluid viscosity were more prevalent for the transition from the moving bed flow to the heterogeneous suspension, while for the stationary to the moving bed, it was more discreet. The water was unable to achieve the heterogeneous suspension, probably due to the particle shape. The bed erosion for lower viscosity fluids happens mostly by the fluid impact over the particle exposed surface. However, the flat-shaped particles' exposed area

is too small for the water to suspend it properly. Thus, fluids with higher viscosities performed better on the particle suspension since the bed erosion was developed through shear effects.

Finally, a correlation was developed based on the flow pattern map data, aiming the biphasic pressure drop determination as a function of ν and Re, employing a single correlation. The correlation provided a satisfactory agreement with the experimental data.

The viscosity effects on the flow pattern transition were studied through the correlation and it was observed that, as the viscosity was increased, the Δp and u_m requirement for the heterogeneous suspension flow achievement was decreased. The statement is especially relevant for applications in which pipeline integrity is at risk. Similarly, the power consumption required to achieve the suspension is decreased as the fluid viscosity is increased.

5.1. Suggestion for Further Work

For biphasic liquid-solid flows, the following topics can be considered for further studies:

a) Experimental evaluation of fluids with different values of ν, aiming to validate the proposed correlation or provide a more precise correlation

b) Implementation of particle image velocimetry (PIV) technique for flow pattern studies, providing fluid velocity and shear stress profiles for each flow configuration.

c) Combine the effects of fluid dynamic viscosity on flow pattern transition with other parameters, aiming to achieve a more generic correlation. The suggested parameters are the solids concentration, particle diameter, solid to liquid density ratio, and pipeline inclination and diameter.

d) Analyze the influence of specific non-Newtonian rheological properties on the biphasic pressure drop and transition between different flow patterns.

e) Evaluation of flow pattern transition considering the influence of other drilling operational variables such as annular hydraulic diameter and pipeline rotation.

REFERENCES

Aditc, 2015. The Drilling Manual.

Akhshik, S., Behzad, M., Rajabi, M., 2015. CFD-DEM approach to investigate the effect of drill pipe rotation on cuttings transport behavior. J. Pet. Sci. Eng. 127, 229–244. https://doi.org/10.1016/j.petrol.2015.01.017

Amanna, B., Reza, M., Movaghar, K., 2016. Journal of Natural Gas Science and Engineering Cuttings transport behavior in directional drilling using computational fluid dynamics (CFD). J. Nat. Gas Sci. Eng. 34, 670–679. https://doi.org/10.1016/j.jngse.2016.07.029

ANP[1] (2018) Publicações Livreto Upstream. <http://www.anp.gov.br/images/publicacoes/Livreto_Upstream_2018-P.pdf.> Acessado em:1/10/2018.

ANP[2] (2018) Dados abertos da Agência Nacional do Petróleo. <http://www.anp.gov.br/dados-abertos-anp>. Acessado em:1/10/2018.

Bourgoyne, A.T., Milheim, K.K., Chenevert, M.E., Young Jr., F.S., 1991. Applied Drilling Engineering, 2nd ed. Society of Petroleum Engineers.

Brown, N.P., 1991. Flow regimes of settling slurries in pipes. In: Slurry Handling Design of Solid–Liquid Systems, Elsevier, London, pp. 41–52.

Cao, C., Zhao, Y., Dong, S., Guo, Q., 2009. Dimensional similitude for scale-up of hydrodynamics in a gas-liquid-(solid) EL-ALR. Chem. Eng. Sci. 64, 4992–5001. https://doi.org/10.1016/j.ces.2009.08.006

Capecelatro, J., Desjardins, O., 2013. Eulerian-Lagrangian modeling of turbulent liquid-solid slurries in horizontal pipes. Int. J. Multiph. Flow 55, 64–79. https://doi.org/10.1016/j.ijmultiphaseflow.2013.04.006

Cedro RR (2014) A estratégia do pré-sal como política de desenvolvimento nacional. Cadernos do Desenvolvimento, 9:105–117.

Cheng, Y., Zhu, J.-X.J., 2008a. CFD Modelling and Simulation of Hydrodynamics in Liquid-Solid Circulating Fluidized Beds. Can. J. Chem. Eng. 83, 177–185. https://doi.org/10.1002/cjce.5450830204

Cheng, Y., Zhu, J., 2008b. Hydrodynamics and scale-up of liquid-solid circulating fluidized beds: Similitude method vs. CFD. Chem. Eng. Sci. 63, 3201–3211. https://doi.org/10.1016/j.ces.2008.03.036

Colebrook, C. F., Blench, T., Chatley, H., Essex, E.H., Finniecome, J.R., Lacey, G., Williamson, J., MacDdonald, G.G., 1939. Correspondence. Turbulent Flow in Pipes, With Particular Reference To the Transition Region Between the Smooth and Rough Pipe Laws. (Includes Plates). J. Inst. Civ. Eng. 12, 393–422. https://doi.org/10.1680/ijoti.1939.14509

Condolios, E. & Chapus, E. E. 1963 Designing solids-handling pipelines. Chem. Engng 131-138. *apud* Doron and Barnea (1996).Davidson, P.A., 2015. Turbulence, An Introducation For Scientists and Engineering 678.

Dewangan, S.K., Sinha, S.L., 2016. Journal of Non-Newtonian Fluid Mechanics On the effect of eccentricity and presence of multiphase on flow instability of fully developed flow through an annulus. J. Nonnewton. Fluid Mech. 236, 35–49. https://doi.org/10.1016/j.jnnfm.2016.08.008

Doron, P., Barnea, D., 1996. Flow pattern maps for solid-liquid flow in pipes. Int. J. Multiph. Flow 22, 273–283. https://doi.org/10.1016/0301-9322(95)00071-2

Doron, P., Barnea, D., 1995. Pressure drop and limit deposit velocity for solid-liquid flow in pipes. Chem. Eng. Sci. 50, 1595–1604. https://doi.org/10.1016/0009-2509(95)00024-Y

Doron, P., Barnea, D., 1993. A three-layer model for solid-liquid in horizontal pipes. Int. J. Multiph. Flow 19, 1029–1043.

Doron, P., Granica, D., Barnea, D., 1987. Slurry flow in horizontal pipes-experimental and modeling. Int. J. Multiph. Flow 13, 535–547. https://doi.org/10.1016/0301-9322(87)90020-6

Duan, M., Miska, S.Z., Yu, M., Takach, N.E., Ahmed, R.M., Zettner, C.M., 2008.

Transport of Small Cuttings in Extended-Reach Drilling. SPE Drill. Complet. 23, 258–265. https://doi.org/10.2118/104192-PA

Durand, R. 1953 Basic relationships of the transportation of solids in pipes experimental research. In Proc. 5th Minneapolis Int. Hydraulics Convent., Minneapolis, Minn., pp. 89-103. *apud* Doron and Barnea (1987).

Faddick, R., 1970. The hydraulic transportation of solids in pipelines. Montana State University.

Fox, R.W., McDonald, 2011. Introduction to Fluid Mechanics, Neurology. https://doi.org/10.1212/WNL.0b013e3182315259

Fox, R.W., Pritchard, P.J., McDonald, A.T., 2009. Introdução à Mecanica dos Fluidos, 7th ed. LTC - Livros Técnicos e Científicos Editora Ltda.

Freitas AGB de, Santana CR, Silva R da P, Silva GF da (2007) Investigação das facilidades e métodos utilizados atualmente no processamento primário de petróleo em campos onshore e offshore. 4º PDPETRO, 1–8.

Ghasemikafrudi, E., Hashemabadi, S.H., 2016. Numerical study on cuttings transport in vertical wells with eccentric drillpipe. J. Pet. Sci. Eng. 140, 85–96. https://doi.org/10.1016/j.petrol.2015.12.026

Gillies, R.G., Shook, C.A., Wilson, K.C., 1991. An improved two layer model for horizontal slurry pipeline flow. Can. J. Chem. Eng. 69, 173–178. https://doi.org/10.1002/cjce.5450690120

Gillies, R. G., W. H. W. Husband and M. H. Small, “A Study of Flow Conditions Arising in Horizontal Coarse Slurry Pipe- line Practice. Phase I”, Report R-832-2-C-85, Saskatchewan Research Council, Saskatoon, Sask. (1985).

Glicksman, L.R., 1984. Scaling Relationships for Fluidized Beds 1373–1379.

Glicksman, L.R., Hyre, M.R., Farrell, P.A., 1994. Dynamic similarity in fluidization. Int. J. Multiph. Flow 20, 331–386. https://doi.org/10.1016/0301-9322(94)90077-9

Han, S.M., Hwang, Y.K., Woo, N.S., Kim, Y.J., 2009. Solid-liquid hydrodynamics in a slim hole drilling annulus. J. Pet. Sci. Eng. 70, 308–319.

https://doi.org/10.1016/j.petrol.2009.12.002

Hemphill, T., Ravi, K., 2006. Pipe rotation and hole cleaning in an eccentric annulus. SPE/IADC Drill. Conf. Proc. 1061–1065.

Hopkin, E. a., 1967. Factors Affecting Cuttings Removal During Rotary Drilling. J. Pet. Technol. 807–814. https://doi.org/10.2118/1697-PA

Hussaini, S., Azar, J., 1983. Experimental Study of Drilled Cuttings Transport Using Common Drilling Muds. Soc. Pet. Eng. J. 23, 11–20. https://doi.org/10.2118/10674-PA

Kelessidis, V.C., Bandelis, G.E., 2005. Flow Pattern Transitions and Flow Pattern Detection of Dilute Solid–Liquid Mixtures in Horizontal Concentric and Eccentric Annulus, in: 7th World Congress of Chemical Engineering. Glasgow.

Kloss, C., Goniva, C., Aichinger, G., Pirker, S., 2009. Comprehensive DEM-DPM-CFD Simulations-Model Synthesis, Experimental Validation and Scalability, in: Seventh International Conference on CFD in the Minerals and Process Industries. pp. 1–7. https://doi.org/10.1039/c5cp04203h

Larsen, T.I., Pilehvari, A. a., Azar, J.J., 1997. Development of a New Cuttings-Transport Model for High-Angle Wellbores Including Horizontal Wells. SPE Drill. Complet. 12, 129–135. https://doi.org/10.2118/25872-PA

Lockett, T.J., Richardson, S.M., Worraker, W.J., 1993. The Importance of Rotation Effects for Efficient Cuttings Removal During Drilling, in: SPE/IADC 25768 - SPE/IADC Drilling Conference. Amsterdam.

Martins, A.L., Sa, C.H.M., Louren, A.M.F., Campos, W., 1996. Optimizing Cuttings Circulation In Horizontal Well Drilling, in: SPE 35341 - Petroleum Conference & Exhibition of Mexico. Villahermosa, Mexico, pp. 295–304.

Miedema, S.A., Ramsdell, R.C., 2016. Slurry Transport Fundamentals, a Historical Overview & The delft Head Loss & Limit Deposit Velocity Framework, Pengaruh Harga Diskon Dan Persepsi Produk Terhadap Nilai Belanja Serta Perilaku Pembelian Konsumen.

Natarajan, P., Velraj, R., Seeniraj, R. V., 2014. Hydrodynamic similarity in liquid-solid circulating fluidized bed risers. Powder Technol. 264, 166–176. https://doi.org/10.1016/j.powtec.2014.05.027

Nazari, T., Hareland, G., Azar, J.J., 2010. Review of Cuttings Transport in Directional Well Drilling: Systematic Approach, in: SPE 132372 - Western Regional Meeting. Anaheim, California. https://doi.org/10.2118/132372-MS

Newitt, D. M., J. F. Richardson, M. Abbott and R. B. Turtle. “Hydraulic Conveying of Solids in Horizontal Pipes”, Trans. Inst. Chem. Eng., 33, 93-1 13 (1955). *apud* Gillies et al. (1991).

Palacios, F. Estudo experimental do escoamento de fluido newtoaniano em contração abrupta axissimétrica com a técnica de velocimetria por imagem de partículas. Federal University of Technology-Paraná, 2011.

Panton, R.L., 2013. Incompressible Flow, John Wiley & Sons, Inc., Hoboken, New Jersey.

Peker, S.M., Helvaci, S.S., 2011. Solid-Liquid Two Phase Flow.

Pope, S.B., 2000. Turbulent Flows. J. Turbul. 1, 771. https://doi.org/10.1088/0957-0233/12/11/705

Ragouilliaux, A., Herzhaft, B., Bertrand, F., Coussot, P., 2006. Flow instability and shear localization in a drilling mud. Rheol. Acta 46, 261–271. https://doi.org/10.1007/s00397-006-0114-2

Sayindla, S., Lund, B., Ytrehus, J.D., Saasen, A., 2017. Hole-cleaning performance comparison of oil-based and water-based drilling fluids. J. Pet. Sci. Eng. 159, 49–57. https://doi.org/10.1016/j.petrol.2017.08.069

Turian, R.M., Yuan, T. -F, 1977. Flow of slurries in pipelines. AIChE J. 23, 232–243. https://doi.org/10.1002/aic.690230305

Walker, S., Li, J., 2000. The Effects of Particle Size, Fluid Rheology, and Pipe Eccentricity on CuttingsTransport, in: SPE 60755 - SPE/ICoTA Coiled Tubing Roundtable. Houston, Texas, pp. 1–10.

White, F., 2010. Fluid Mechanics. McGraw-Hill, New York 862. https://doi.org/10.1111/j.1549-8719.2009.00016.x.Mechanobiology

White, F.M., 1976. Viscous Fluid Flow.

Williams, C.E., Bruce, G.H., 1951. Carrying Capacity of Drilling Muds. J. Pet. Technol. 3, 111–120. https://doi.org/10.2118/951111-G

Yarin, L.P., 2012. The Pi-theorem: Applications to fluid mechanics and heat and mass transfer, The Pi-Theorem: Applications to Fluid Mechanics and Heat and Mass Transfer. https://doi.org/10.1007/978-3-642-19565-5

Yeckel, A., Middleman, S., 1987. Removal of a viscous film from a rigid plane surface by an impinging liquid jet. Chem. Eng. Commun. 50, 165–175. https://doi.org/10.1080/00986448708911823

APPENDIX A – DIMENSIONS CALCULATION

The values of pipeline internal diameter, slurry critical velocity, and fluid viscosity were assumed as project requirements to estimate the dimensions and equipment employed in the experimental bench,. The requirements chosen were the viscosity of the water-glycerin 60%wt mixture, $\mu_c = 10^{-2}$ Pa.s, the critical velocity of $u_{s\_critical} = 4$ m/s and internal diameter of D = 36 mm.

It was necessary to determine the flow development length and the fluid's pressure to achieve the critical velocity to select the thickness of the pipeline and the pump necessary to pressurize the system.

The pressure loss due to friction effects is given by Fox et al. (2011) as a function of the friction factor f, pipeline total length L_{total} and internal diameter d, fluid specific mass ρ and critical velocity $u_{s\_critical}$, as shown in Equation (38).

$$\Delta p = f \frac{L_{total}}{d} \rho \frac{u_{s\_critical}^{2}}{2} \tag{38}$$

The pressure drop determination procedure is the same for the pressure transducers' specification and the helicoidal pump. The only parameter changing is the equivalent length between the points where the pressure is measured, $L_{total.}$

The friction factor determination for turbulent flows can be developed by the Colebrook correlation, given in Equation (39), as a function of the pipeline roughness ratio e/D and Reynolds number (Fox and McDonald, 2011).

$$\frac{1}{\sqrt{f}} = -2.0 \log\left(\frac{e/d}{3.7} + \frac{2.51}{\mathrm{Re}\sqrt{f}} \right) \tag{39}$$

The determination of f through Colebrook's correlation must be developed through an iterative method, which implies in a first value stipulation. The value employed for the first iteration was calculated through Haaland's correlation (Fox and McDonald, 2011), shown Equation (40).

$$\frac{1}{\sqrt{f}} = -1.8\log\left(\left(\frac{e/d}{3.7}\right)^{1.11} + \frac{6.9}{\mathrm{Re}}\right) \quad \textbf{(40)}$$

After the first estimative for the friction factor, the value was determined using the iterative method with an error of close to 1%.

The next step consisted of the determination of the pipeline length between the measurement points. The parameter will be determined individually for the test section estimation and the pump selection.

i) Pressure drop in the test section

The estimative for the pressure drop in the test section had the objective of selecting the pipeline diameter. Therefore, the estimative accounted for three diameters D = 26 mm, 36mm and 49 mm for L_{total} = 3 m. The curves resultant from this estimative are shown in Figure 10, Section 3.2.3, where the pipeline's choice with D = 36 mm is detailed.

ii) Pump Selection

The determination of the pipeline total length L_{total}, which included the nominal length L and the equivalent length of pressure drop elements in the flow loop, L_e. The length considered for the calculation is shown in Table 14, in which it is possible to see that the values of pipeline length and the number of elements in the flow loop are over-dimensioned to provide a safety margin. Also, the value employed for the pressure drop determination was of L_{total} = 32 m.

Table 14 – Pressure drop elements in the experimental setup, the equivalent length associated with each component, and the equivalent length's total value.

	Number of elements	L_e
Standard Elbow 90º	4	6
Standard tee flow through a branch	2	3
Ball Valve	4	3
Pipeline Length	-	18
L_{total} **[m]**	**30**	

(Source: author)

Based on the procedure described, it is required around Δp_{pump} = 3.3 bar for the water-glycerin 60%wt to achieve Q = 8 m³/h. A commercial plexiglass pipe with internal diameter D = 25 mm and thickness t = 3 mm was employed, and its resistance is around 3.5 bar, which is in agreement with project requirements.

APPENDIX B – UNCERTAINTIES DETERMINATION

Three measuring devices will be employed over the experiments: a *Coriolis* mass flow meter, in which the volumetric flow rate and particle concentration will be determined, a pressure transducer, and a pachymeter to determine the pipeline diameter.

Each value measured by the different devices will be associated with an aleatory uncertainty, to which the value is dependent on its constructive characteristics and is suggested by the manufacturer. The values of the Type B uncertainties for each device are show in Table 15.

Table 15 – Type B uncertainties of the measuring devices employed in the present work.

Device	Standard Uncertainty
Coriolis mass flow meter	± 0.5%
Pressure transducer	± 0.41%
Pachymeter	± 0.02 mm

(Source: author)

As shown in Table 15, the pressure transducer and Coriolis mass flow meter uncertainties are percentages of the value measured.